MINIATURIZED FIBER OPTIC TRANSMISSION SYSTEM FOR MAGNETIC RESONANCE IMAGING SIGNALS

A THESIS

SUBMITTED TO THE DEPARTMENT OF ELECTRICAL AND

ELECTRONICS ENGINEERING

AND THE INSTITUTE OF ENGINEERING AND SCIENCE

OF BILKENT UNIVERSITY

IN PARTIAL FULFILLMENT OF THE REQUIREMENTS

FOR THE DEGREE OF

MASTER OF SCIENCE

By

Ömer Gökalp Memiş

July, 2005

I certify that I have read this thesis and that in my opinion it is fully adequate, in scope and in quality, as a thesis for the degree of Master of Science.

Prof. Dr. Ergin Atalar (Co-Supervisor)

I certify that I have read this thesis and that in my opinion it is fully adequate, in scope and in quality, as a thesis for the degree of Master of Science.

Prof. Dr. Orhan Aytür (Co-Supervisor)

I certify that I have read this thesis and that in my opinion it is fully adequate, in scope and in quality, as a thesis for the degree of Master of Science.

Prof. Dr. Ayhan Altıntaş

I certify that I have read this thesis and that in my opinion it is fully adequate, in scope and in quality, as a thesis for the degree of Master of Science.

Asst. Prof. Dr. Vakur B. Ertürk

I certify that I have read this thesis and that in my opinion it is fully adequate, in scope and in quality, as a thesis for the degree of Master of Science.

Dr. Tarık Reyhan

Approved for the Institute of Engineering and Science:

Prof. Dr. Mehmet B. Baray
Director of the Institute

ABSTRACT

MINIATURIZED FIBER OPTIC TRANSMISSION SYSTEM FOR MAGNETIC RESONANCE IMAGING SIGNALS

Ömer Gökalp Memiş
M.S. in Electrical and Electronics Engineering
Supervisors: Prof. Dr. Ergin Atalar and
Prof. Dr. Orhan Aytür
July, 2005

In conventional Magnetic Resonance Imaging (MRI) instruments, after echo signals are received by an MRI coil, they are transmitted through an ultra low noise transmission system consisting of electrical cables. Although this design proved to be effective over the years, there are recent developments in the MRI technology which require a better, more sophisticated design. One of these emerging technologies is "parallel imaging", where total size of interconnections is the primary problem, and the other is "interventional MRI", where safety needs to be improved. The *Miniature Fiber Optic Transmission System* was developed to serve these needs. The system consists of a receiver MRI coil with passive detuning, a two-stage low-noise preamplifier and a low-noise laser diode connected to a photodetector with fiber optic cable in between. The overall noise figure of the system is measured to be lower than 1 dB which guarantees that total signal-to-noise ratio (SNR) reduction in the images due to optical MRI signal transmission system is less than 15%. Total power consumption is 50mW and the device is switchable by another fiber optic line, which can also control active detuning circuit if it is present. A prototype device was tested in a GE 1.5 Tesla MRI instrument and several images were acquired with a slight SNR drop, due to problems with passive detuning. We believe that this design will significantly reduce the size of parallel imaging arrays and enable placement of internal coils into body cavities without providing any safety hazard to the patient, such as electrical shock or burns.

Keywords: Magnetic Resonance Imaging, Fiber Optics, Laser, Interventional Imaging, Parallel Imaging, Ultra Low Noise System.

ÖZET

MANYETİK REZONANS GÖRÜNTÜLEME SİNYALLERİ İÇİN MİNYATÜR FİBER OPTİK İLETİM SİSTEMİ

Ömer Gökalp Memiş
Elektrik Elektronik Mühendisliği, Yüksek Lisans
Tez Yöneticileri: Prof. Dr.Ergin Atalar ve
Prof. Dr. Orhan Aytür
Temmuz, 2005

Geleneksel Manyetik Rezonans Görüntüleme (MRG) aygıtlarında, yankı sinyalleri MRG bobini tarafından yakalandıktan sonra aşırı düşük gürültülü koaksiyel kablolar aracılığıyla iletilir. Bu tasarım işe yararlılığını kanıtlamıştır; ama MRG teknolojilerinde daha iyi, daha karmaşık bir tasarım gerektiren yeni gelişmeler olmaktadır. Ortaya çıkan bu teknolojiler, arabağlantıların boyutunun öncelikli problem olduğu "paralel görüntüleme" ve güvenliğin arttırılması gereken "girişimsel görüntüleme"dir. *Minyatür Fiber Optik İletim Sistemi* bu gereksinimleri karşılamak için geliştirilmiştir. Önerilen sistem, pasif ayar bozuculu bir alıcı bobin, iki katlı düşük gürültülü bir güçlendirici ve fiber optik kablo aracılığla fotoalıcıya bağlanmış düşük gürültülü bir lazer diyottan oluşmaktadır. Sistemin gürültü figürü $1dB$'nin altındadır; ki bu da optik MRG sinyal iletim sistemindan dolayı sinyal-gürültü oranındaki (SGO) kaybın %15'ten az olduğunu garantiler. Toplam güç tüketimi $50mW$'tır ve aygıt başka bir fiber optik hat üzerinden anahtarlanabilir, bu hat eğer varsa aktif ayar bozucuyu da kontrol edebilir. Prototip cihaz, MRG aygıtında test edilmistir ve görüntü alınmıştır: Pasif ayar bozucudan kaynaklanan bir problemden dolayı SGO'su beklenenden biraz düşüktür. Bu tasarımın, paralel görüntüleme dizisinin boyutunu ciddi olarak düşüreceğine ve içsel bobinlerin güvenlik tehlikesi (yanıklar, elektrik çarpması) olmaksızın vücut boşluklarına girmesine olanak vereceğine inanmaktayız.

Anahtar sözcükler: Manyetik Rezonans Görüntüleme, Fiber Optik, Lazer, Girişimsel Görüntüleme, Paralel Görüntüleme, Aşırı Düşük Gürültülü Sistem.

To my parents...

Contents

List of Figures

List of Tables

Chapter 1

Introduction

1.1 Motivation and Literature Survey

Fiber optics is the technique of using coherent or incoherent light through confining it in waveguide fibers. Fiber optics has been available for a long time, and has found its place in many applications in electrical and biomedical engineering; however little effort has been spent to integrate fiber optics into Magnetic Resonance Imaging (MRI). Considering what fiber optics have to offer, it can expand the horizons of MRI, proving further reach, better safety and smaller sized devices.

The primary motivation for this project was to construct an optical system capable of transmitting magnetic resonance signals with the highest signal-to-noise ratio (SNR). This would make a miniaturized internal (endoluminal) MRI coil possible, without sacrificing the safety of patient. Recently, another possible area which would benefit from a small sized fiber optical transmission system has also emerged: multiple-channel or parallel imaging.

Internal MRI coils have been developed for many years. They offer different sizes for several applications: intravascular [1, 2], transesophageal [3], endourethral [4] and endorectal/transrectal coils [5, 6]. The main reason for the

interest in such devices is their ability to probe into the body further than external coils, yielding better SNR in the regions of interest.

Safety of the patient in magnetic resonance imaging is a criterion defined by international standards and given upmost importance. Although interventional prototypes have been available for some time, the potential risks they pose to the patient have somewhat limited their widespread usage and forbade their clinical use. Several work has been done to better analyze and estimate the actual risk, which is primarily the problem of radiofrequency (RF) heating. RF heating stems from the interactions of the electromagnetic field with the metallic parts of the interventional device (ferromagnetic or nonferromagnetic). Given the proximity of the interventional device to local tissue, potential hazards of this kind of heating is a concern not to be underestimated. Currently it has been identified that tip of the wires are the regions where highest heating occurred, although the amount of heating is a complex function of orientation and length factors [7–9]. Moreover, models involving specific absorbtion rate (SAR) and bioheat transfer equation are created [10] to better estimate the heating process.

Theoretical and experimental work on the heating around coaxial cables show that the heating can be lowered by limiting the size of coaxial sections and using chokes to interconnect these sections [11]. While this proves to decrease the heating, it is also shown that chokes themselves created new resonant fields with concentrated electric fields. Recently Weiss et al. have proposed using transformers in between coaxial cable sections and have developed a safer coaxial transmission line [12]. Yet these safe coaxial cable designs are still being investigated for clinical use.

The idea of using fiber optics instead of coaxial cables in magnetic resonance imaging is a solution for this RF heating problem. Since the fiber itself forms a nonconductive path, it does not create excessive heat around its tips and it does not have resonant sections where fields become concentrated. Thus, for the concern of interventional device safety, using fiber optic cables for connections will yield less risk.

In fact, the idea of using fiber optics have already been proposed as a safer

alternative in a different context: MR-guided interventional operations. During MR-guided interventional operations, tracking and localization of catheters and devices are crucial for success, for which passive and active methods are used. Summarizing, passive methods use the artifacts generated from interventional device and have disadvantages of relatively low spatial resolution and reduced speed compared to active methods [13]. On the contrary, active methods involve tuned RF coils and thus require dedicated detuning mechanism usually in the form of leads and cables which in turn suffers from the RF heating problem. One solution that combined the benefits of active tracking with the safety of the passive one is a wireless detuning system by Wong et al. [14]. Their work suggested using a fiber pigtailed photoresistor for lowering the Q of the system and detuning the coil when necessary; thereby eliminating the need for electrical connections.

Besides the safety factor, there is another field which would greatly benefit from fiber optic cabling, parallel imaging. Similar to the rapid growth of interventional methods in MRI, multiple channel imaging seems as another rapidly emerging subarea. In a recent conference (ISMRM'05) several researchers have presented papers of a 32-channel head coil [15], 48-channel body/spine coil [16] and even a 96-channel MRI system [17], which can be interpreted as the signs of prospective MRI systems with large number of channels, commercially available.

The fusion of fiber optic technologies with these new extreme multiple channel systems can result in a better MRI scanner. Using fibers can eliminate some of the drawbacks of the current systems, such as the size of the bundle of coaxial cables or the safety issues with this bundle. A recent proposal featured an optical interconnect for multiple channel MRI systems [18] which is similar to what we have proposed at ESMRMB'03 [19] and have been developing since. Although the main idea in these papers are the same, the technologies employed are different. Koste et al. used a fiber optic modulator where we have chosen a low-noise laser diode instead to couple the MRI signals to laser. Both technologies offer the benefits of fibers: First, they do not contain coaxial cables, therefore risks of electrical shock or RF burns are nonexistent. Second, since they are immune to the electrical interference coaxial cables experience, the noise contributed by the

nearby electronics (mainly from the switching) and with the nonconductive path, they are free of any unbalanced current or potential common ground problems. Last but not the least, the use of fibers in a 96-channel MRI system will yield significant size reductions in the interconnect region between the scanner hardware and the controller/receiver hardware. Although these might seem practical problems, their existence might as well be the limit in the realization of commercial multiple channel scanners.

1.2 The Objective and Scope of the Thesis

This thesis describes the design and implementation of a prototype device to be used in Magnetic Resonance Imaging. The device incorporates a optical fiber which is the primary means to transmit the MR signals. Real-time electrical to optical and optical to electrical conversion systems together with ultra-low noise amplifiers are in the core of this transmission system, and the connection between coil and MRI instrument is nonconductive. Furthermore, preservation of SNR of the original signal during transmission is the main aim of the system.

The thesis is divided into chapters, Chapter 1 contains the introduction and motivation. Chapter 2 goes into the the theory of noise and possible sources. In Chapter 3, the whole design is described in parts and in whole with complete schematics and parameters. Chapter 4 presents the simulation results obtained in Orcad Pspice 9.2.3 and Ansoft Designer SV 1.0. Following the simulations Chapter 5 contains the experimental results: laboratory measurements and the image acquisitions from Magnetic Resonance Instruments. At the end, Chapter 6 contains the discussions regarding this work and conclusions.

The Appendices contain additional information: Appendix A shows a methodology to measure noise figure with the use of a calibrated noise source and a means to measure power. Appendix B contains the matching parameters and calculations. Appendix C and D presents the manufacturer datasheet of the transistor BFP420 and the datasheet of one of the custom made laser diodes.

Chapter 2

Theory

The most important aspect of this design is to preserve the signal-to-noise ratio as much as possible. MRI signals can be extremely low power signals and they should be transmitted with the addition of minimal noise. Throughout the operation of our prototype system, there are several types of noise encountered.

The three different kinds of noise to be accounted for and dealt with are *Thermal Noise*, *Shot Noise* and *Laser Intensity Noise*. Thermal noise is created by ohmic resistances, shot noise is created by the quantum nature of current carriers (electrons) and laser intensity noise is created by the laser diode of the transmitter.

2.1 Thermal Noise

Thermal noise is generated by the thermal agitation of electrons together with the interactions between them and it is highly dependent on the kinetic energies of electrons, the average of which is proportional to absolute temperature. The power of this noise is also proportional to the bandwidth over which the noise is measured.

The formula for the available thermal noise power from a resistor on a matched

load is

$$P_{th} = k_B T B, \tag{2.1}$$

where T is the absolute temperature, B is the bandwidth expressed in hertz and k is the Boltzmann's constant. Sometimes the value for room temperature (290 K) is expressed as

$$P_{th} = -174 dBm/Hz, \tag{2.2}$$

which should be multiplied with the bandwidth to find the actual noise power.

In the design, thermal noise is generated by all amplifiers and semiconductors which have resistance. However, in practice it is more important when the MRI signal level is close to the level of thermal noise, although its power is same for every resistance. After the amplification, power of the MRI signal gets further away from the thermal noise level and is less affected by this noise.

2.2 Shot Noise

In the general sense, shot noise comes from the discreteness of current carriers in conductors and resulting statistical variations over time. Since electron hole pairs (EHPs) in the photodetector is generated by incoming light, it might be better to redefine the shot noise according to that fact: Optically speaking, shot noise is produced by the quantum nature of photons (and consequential electrons) arriving at the detector and related detection statistics. Power of the resulting noise is related directly to the amount of average current passing through and therefore corresponding light incident on the photodetector. The power spectral density is characterized by a white noise spectrum. In contrast to thermal noise, shot noise cannot be eliminated by lowering the temperature.

The power for shot noise per Hertz is

$$P_{shot} = 2 e I_{DC} R_L, \tag{2.3}$$

where e is the electron charge, I_{DC} is the average current and R_L is the resistance on which shot noise power is calculated. A better formula, taking into account

the photodetection process is [20]

$$P_{shot} = 2e(\frac{\eta e}{h\nu}P_{opt})R_L = \frac{2e^2\eta R_L}{h\nu}P_{opt}, \tag{2.4}$$

where I_{DC} is replaced with the formula of equivalent optical power P_{opt}. In this formula, η is the quantum efficiency of photodetector and ν is the frequency of the light.

In the photodetection process, optical power is transmitted into electrical power and a current is consisting of optically generated EHPs in semiconductor photodiode. The shot noise level, compared to thermal noise, is several orders more. Preamplification is required to make MRI signals more than this shot noise level.

2.3 Laser Intensity Noise

The third noise source, which turns out to be the dominant one during optical transmission, is the Laser Intensity Noise (LIN). It is caused by intensity fluctuations due primarily to spontaneous light emission. Also the presence of external feedback or reflections into the laser will contribute to this noise and increase its power. RIN (Relative Intensity Noise), the ratio of noise power to average power, is used to express the intensity noise. RIN is a dynamic range measurement: It depends on the average power of the optical beam. The formula for RIN is

$$RIN = 10log\Big(\frac{< P_{opt}^2 >}{P_{opt}^2}\Big), \tag{2.5}$$

where $< P_{opt}^2 >$ is the mean square average LIN power and P_{opt}^2 is the average optical power squared. Notice that output power and operating current have a linear relationship and the proportionality constant is Γ_{LD} - responsivity as

$$P_{opt} = \Gamma_{LD} I_0. \tag{2.6}$$

This relationship also applies to noise power and noise current, therefore the

noise power due to laser intensity noise on a resistance R_L is

$$< I_{RIN} >^2 = 10^{RIN/10} I_0^2, \tag{2.7}$$

$$P_{LIN} = R_L < I_{RIN} >^2 = 10^{RIN/10} I_0^2 R_L, \tag{2.8}$$

where I_0 is the current at which the laser diode is operated and R_L is the resistance upon which noise is measured.

LIN effects the transmitted signal during electro-optical conversion when the amplified MRI signals are coupled to the laser. Again, the preamplification is required to make SNR degradation minimal.

Chapter 3

Materials and Methods

Looking at an MRI system, the basic operation scheme is:

- The transmitter coil emits the electromagnetic wave responsible for excitation of the sample.
- The excited sample reradiates the electromagnetic wave which is captured by the receiver coil, thereby forming the MR signals.
- Passing through an ultra-low-noise preamplifier (ULNA), the power of received signals increase, becoming significantly greater than noise introduced in the later stages.
- The boosted signal then gets processed by the MRI scanner, yielding the final image.

Naturally, the usage of fiber-optic technologies would require addition of new circuitry to current ones. However, care must be taken while designing, as MRI compatibility is an extremely important issue.

There were some points we have considered throughout the design stage. While most come from the limitations posed by magnetic resonance technology itself, there are other limitations due to currently available commercial products and safety:

1. The main and most important limitation is the prohibition of some materials in magnetic resonance imaging: Ferromagnetic materials, which have a large and positive susceptibility to an external magnetic field [21], exhibit a strong attraction to magnetic fields. Since MR imaging heavily depends on the fundamental properties of nuclear spin under a strong magnetic field, ferromagnetic materials in MRI pose serious hazards to the patient, operator and scanner, primarily due to the strong force ferromagnetic materials experience in the superconductive magnet. MRI-safe materials are paramagnetic materials (typically considered nonmagnetic), which are slightly attracted by external field, and diamagnetic materials, which are slightly repelled.

   Besides the force experienced, highly magnetic materials also create additional problems. First problem is the disturbance of the magnetic field inside MRI magnet. Leading to artifacts and image quality degradation, the loss of uniformity of the field inside MRI chamber is not be underestimated. However, the disturbance decreases with increasing distance from the magnetic material, which suggests that moderately magnetic materials away form the sample will not affect the image, provided that they undergo a weak force and they could be physically stabilized.

   Another problem associated with highly magnetic materials is related to their operation under strong magnetic fields. In electronics, ferromagnetic cores are commonly used in inductors to achieve higher coupling and larger inductance values. Although they suggest small sizes, these cores are subject to magnetic saturation in their core, which significantly decrease their inductance, distorting or even preventing proper operation of the overall circuit. Air-core inductors are safe in regard of magnetic saturation and are essentially MRI-compatible. Furthermore, optical components sensitive to magnetic fields exist: optical isolators, common in low-noise lasers, are composed of two polarizers and a Faraday rotator, whose operation is highly dependent on the magnetic field parallel of the direction of light propagation. Elimination of these components are greatly advised, as they behave

erratically under strong external field.

2. Noise factor and SNR is another limitation in Magnetic Resonance Imaging. Power of the MR signals, when received by coil, is weak in nature. Therefore it is essential that the noise contribution while transporting and processing the signals is kept at a minimum, and several points can be exercised in the design for this purpose:

   First, the usage of ULNAs are essentially required to boost the signal away from the noise level. ULNAs are typically placed as first-stage amplifiers and they are designed for a lowest-noise match rather that the common maximum-power match techniques. Following the ULNA, low-noise amplifiers (LNAs) are cascaded as high-gain stages before any optical conversion takes place. For the lowest noise, the total gain available in these amplifiers should be as high as possible for preventing the possible SNR decrease in later stages. However, there are problems associated with very high gain like the possible compression or saturation of amplifiers and increased nonlinearities in the electrical-optical-electrical (E-O-E) conversion process.

3. Although not a strict requirement, the small size of the device will be a great advantage. In interventional imaging, the size of the device is a limiting factor in its suitability for an application. Intravascular applications require extremely small devices, endoscopic operations use moderately sized ones whereas endorectal imaging can accommodate larger devices. Moreover, small sized devices present less burden to the patient, which is desirable. The other application, parallel imaging, also benefits greatly from the size reduction for the obvious reason of the smaller volume and less mass of the receiver array in a 32+ channel system.

4. A constraint similar to size is power. The design should consume the least power possible, due to three major reasons: battery capacity, heating and primarily in parallel imaging: total power consumption.

   The battery capacity is a physical limit on the duration of operation of

any battery-powered device and as a fact of correlation, smaller sized devices tend to have smaller batteries. Therefore the miniature fiber-optic probe is designed to work with a minimal power consumption of 16mA and 3V, which would enable several hours of operation with 3V, 25mAh or 50mAh lithium batteries.

A second problem related to power consumption is the resulting heat. The power supplied to the device is converted to either RF power through amplification, to optical power via the laser diode or eventually to heat by the circuitry. This heat inherently gets conducted to the nearby tissues or regions. Minimizing the power consumption is needed to decrease this problem since heating is an important safety concern in interventional MR Imaging. One advantage of the heating in optical probe over conventional RF heating common in MRI is the spread of the generated heat over a larger volume. This results in a smaller temperature increase although the amount of transferred heat may be more.

The last problem is the total power consumption in a parallel imaging system. Although a single fiber optic probe requires a small amount of power ($\sim$50mW); on the worst (most inefficient) case where each channel requires a separate fiber optic diode and line, the total power consumption of a $\sim$100-channel will be feasible but high. Moreover, each additional increase in power consumption will result in a significant rise in total. Here the minimization of power consumption is recommended again.

The fiber-optic prototype was designed based on these requirements and recommendations. It consists of the following sections, each of which is either modified or completely new compared to the current designs:

- Coil, together with matching and detuning circuitry
- Transmitter
  - Preamplifier stages

- Laser diode with matching circuitry
- Power and Control circuitry

- Receiver and External Control circuitry

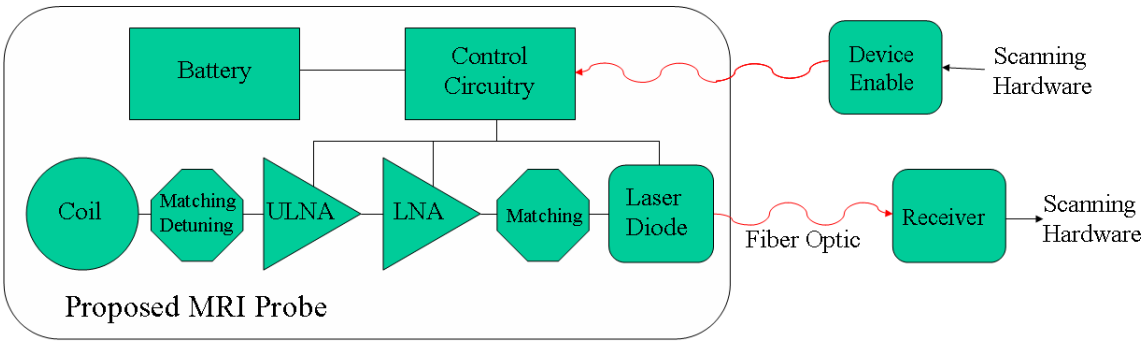

Figure 3.1: Block diagram of fiber optic transmission system: The coil with detuning circuitry, ultra-low-noise preamplifier and laser diode with appropriate matching connected to the receiver. The power is supplied by a battery through the power and control circuitry.

3.1 Coil

The coil is the starting point where electromagnetic echoes of the RF excitation pulse get received and are converted to low power electrical MR signals. The nature of these signals are narrowband VHF; and the center frequency -also called Larmor frequency- is linearly dependent on the main magnetic field by the relationship [22]

$$\omega_0 = \gamma B_0, \tag{3.1}$$

where ω_0 is the center radial frequency, B_0 is the strength of the main DC magnetic field in *Tesla* and γ is the gyromagnetic ratio

$$\gamma = 42.56 \times 10^6 \frac{rad}{T \cdot sec}. \tag{3.2}$$

The bandwidth of these signals are quite low: on the order of 10-100kHz. This eliminates any need for broadband designs, allowing use of simple L-match techniques.

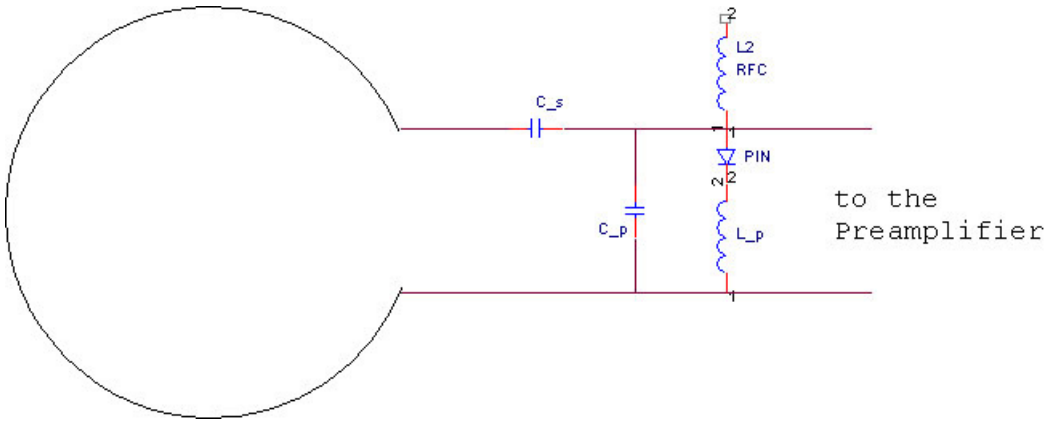

Figure 3.2: Schematics of the coil: A single loop of wire followed by a matching circuitry with active detuning.

As coils work by inductive coupling of electromagnetic waves (time derivative of magnetic flux), they are naturally inductive, even when they are loopless. Thus they need to be matched to the rest of the circuitry both for good power transfer and low noise characteristics.

Based on our observations, a typical single loop coil presented an impedance of about $1\Omega + 25j\Omega$. There are two important things to consider here, first is the angle of this impedance: It is close to 90° or $\frac{\pi}{2}$ which suggests that inductive nature of the coil is dominant, and it can be matched to Z_0 only by capacitive elements. The second point is the real part of the impedance corresponding to the resistance. Although it is the existence of this resistance which permits matching to Z_0; it is also this resistance which increases the noise contribution most. This is the single largest noise source in the overall MR equipment, and unfortunately this noise cannot be eliminated (except possibly by reducing the temperature to absolute zero - 0K). Note that this noise is purely thermal noise.

Using the fact that the impedance is mostly inductive with a small resistance, these coils can be matched to an appropriate Z_0. For convenience Z_0 was taken as 50Ω in our design. 50Ω presented a case in which coil can be matched using only small chipped capacitors rather than bulky inductors: In fact, 2 capacitors in an L-match configuration was enough for this purpose. The exact values of these capacitors can be calculated, however in practice parasitics present a considerable

impedance and it is better to match experimentally by a vector network analyzer or impedance analyzer.

After the matching circuit, there is a second part responsible for *detuning*. Detuning process is responsible for protection of the MR devices, and it effectively makes the receivers (i.e. coils) deaf to the resonant frequency during the RF excitation wave. Detuning circuitry usually consists of special Positive - Intrinsic - Negative (PIN) diodes which can tolerate high power RF signals without going into breakdown [23]. There are two types of detuning: passive and active.

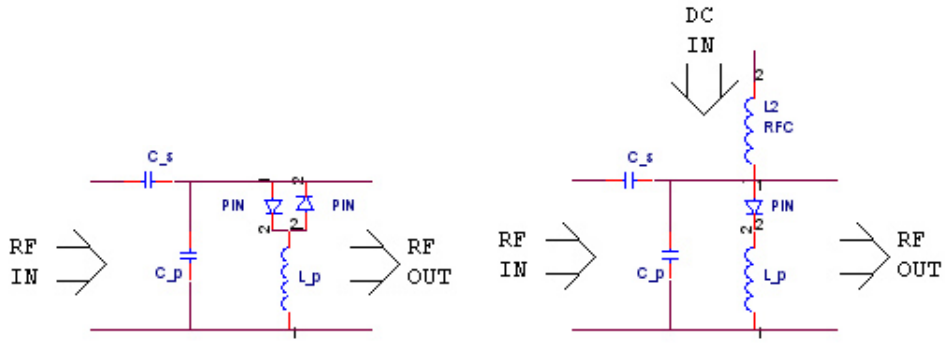

(a) Passive detuning (b) Active detuning

Figure 3.3: Types of detuning: Passive detuning relies on the self-biasing of two back-to-back PIN diodes by incoming high-power RF; whereas active detuning uses an external circuitry for the activation and deactivation of a single PIN diode.

Passive detuning uses two back-to-back PIN diodes in between signal and ground lines to control the delivered power. PIN diodes in this configuration behave as a limiter [24], in which a high-power signal triggers the diodes by injecting minority carriers that eventually decrease the RF impedance of PIN diodes from the order of 10kΩ to 1Ω. The intrinsic region in the middle of PIN diodes results in increased transit time (τ_t) for the carriers and thus slows down the closing of diode - till the injected carriers thermally recombine. During this open period, the low RF impedance reflects most of the incoming high power RF wave, transmitting only a fraction. This procedure presents the following transient for transmitted power:

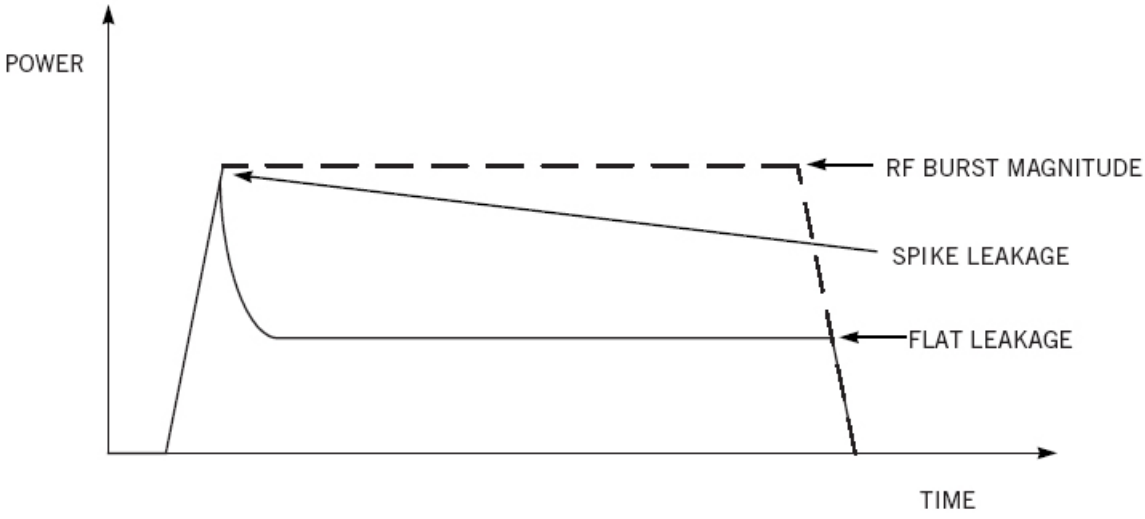

Figure 3.4: Transient for power transfer in passive detuning: Upon activation, PIN diode's RF resistance decreases to several Ohms, reflecting back most of the incoming RF power. Note the spike leakage and flat leakage in this process. Property of EDN, Reed Electronics Group [24]

Note that comparing to the clipper circuits where the signals peak values are limited to V_d or $-V_d$, the limiter circuits act as an attenuator for the whole period once they are activated.

Active detuning differs from passive detuning by the usage of only a single PIN diode and an external control line which supplies current when required. During the period of dead-time, the external current passes through the diode, again decreasing the diode RF resistance and reflecting the high power signal. This turns out to be a better choice for detuning, although extra circuitry is needed: Almost all modern MR scanners use active decoupling to protect their receivers.

Although these methods are applicable, another minor change can extend the effect further: intentional shifting of resonance. Instead of placing the diodes across the signal and ground, they can be placed in series with an inductor whose value is chosen to be the resonant value of either of the matching capacitors. This way, when the PIN diodes are activated (either by passive or active methods) the

capacitor resonates with the inductor and presents a very high impedance to the coil. with this high impedance, the coupling of electromagnetic waves to coil decreases. A more elegant way to implement this idea is using a transmission line to transform the low-impedance of active PIN diodes to the required inductance value [25], as shown in the figure below:

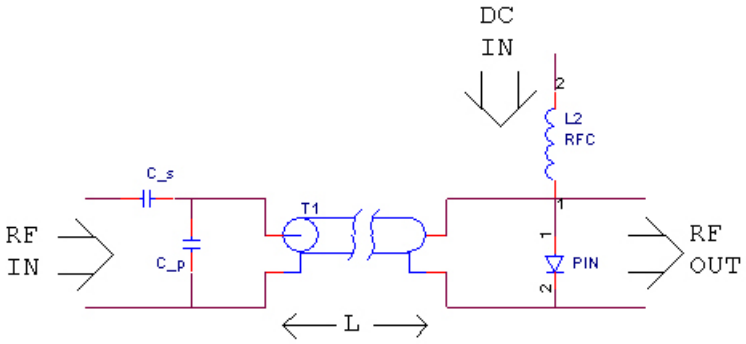

Figure 3.5: Active detuning through a transmission line: The low impedance of the PIN diode is transformed to the inductor value resonant with shunt capacitor.

When driven with current or self-activated through high-power signal, the diode(s) present a low RF resistance which is seen as an inductance through a transmission line of length L. This inductance resonates with the capacitance and yields high-impedance to the coil effectively limiting the coupling to coil and preventing the feed of preamplifiers with a high-power.

A final remark on the design of coils for MR Imaging is to be aware of possible unbalanced currents. These currents typically leak on the outer region of shields of balanced lines such as coaxial cables and they significantly alter the properties of coils, especially the impedance values. Balanced-to-unbalanced converters (Baluns) must be used to prevent unbalanced currents. Note that fiber-optic cables, nonconductive in nature, do not suffer from unbalanced current problems and baluns are not needed in such cases.

3.1.1 Parameters

In our design and experiments, an endorectal coil was used together with appropriate matching and passive or active detuning circuits depending on the experiment.

The endorectal coil was designed as a cylindrical substrate stabilized on a rectangular base. The cylinder had a diameter of 23mm, a length of 143mm and was made of white plastic. The base, which held the matching and detuning circuitry with the connector, had the dimensions of 98mm(L) × 30mm(W) × 5mm(D).

The coil consisted of solid copper wire of 1mm diameter, and it was placed on the surface of the cylindrical plastic, with parallel sides of 136mm on the longitudinal direction of the cylinder and perpendicular sides passing through the whole diameter (23mm) in the axial direction. The whole cylinder -including the coil- was then covered with a heat-shrink tube to ensure safety and isolation from environment.

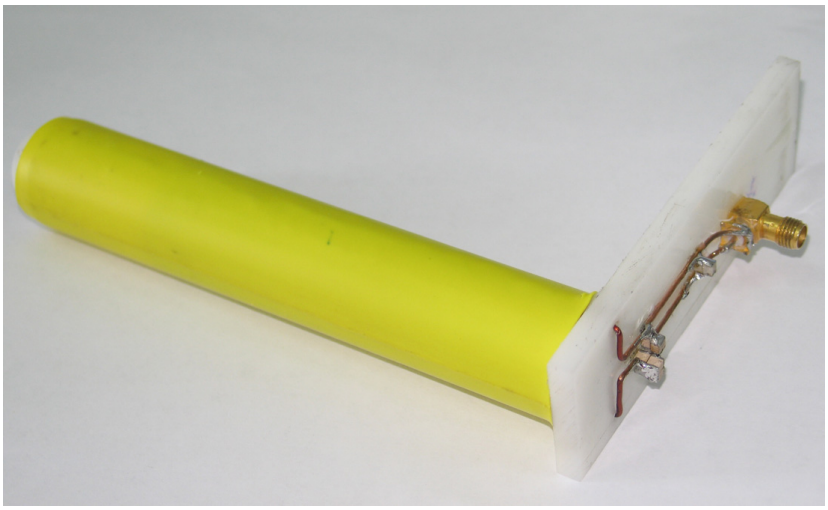

Figure 3.6: Photograph of the coil

The coil was tuned for operation at 63.85Mhz using nonmagnetic chip capacitors by first series configuration then shunt. A wire of length 23mm was placed in between the shunt capacitors and PIN diode(s) which acted as a transmission

line to change the low-impedance values (when PIN diodes are active) to the appropriate resonant inductor. Note that as the coil was matched to $\sim 50\Omega$ with the capacitors, the transmission line did not alter this impedance value seen by the preamplifiers.

The coil was designed to work both as an active or passive detuning device, only by adding or removing a single PIN diode. This was required for comparison purposes, in conventional operation (coaxial cables) the system used active detuning whereas fiber-optic system was experimented with the passive method. This way, resulting images obtained from the MRI receiver were comparable.

3.2 Transmitter

After the weak echoes are captured by the coil, the signals need some basic preprocessing before they can be changed into optical signals. The section of the prototype responsible for preprocessing and optical conversion is the transmitter; and it consists of preamplifiers followed by the laser diode with corresponding bias and match circuitry.

3.2.1 Preamplifier

As stated previously, the intercepted MR signals are extremely low-power, and they have already been affected by the noise contribution from the resistive coil before arriving at preamplifier.

The primary reason to use preamplifiers before any optical conversion is to preserve the SNR as much as possible. To this end, an ULNA must be used as first stages to boost signal, making it much larger than the noise floor in the later stages of device. An ULNA is a special type of amplifier designed to sufficiently high output SNR for a given input SNR such that the noise figure (NF), is lower

than $1dB$. Noise figure is a measure of SNR degradation defined as

$$NF = 10log\left(\frac{SNR_{in}}{SNR_{out}}\right). \tag{3.3}$$

$NF < 1$ means that the output SNR should be at least 0.8 times the input SNR in an ULNA.

Design of an ULNA requires some extra steps compared to the design of an ordinary amplifier. First, the physical limits should be observed: It is impossible to achieve low noise characteristics without proper selection of transistor. In today's wide arsenal of semiconductors, transistors designed for portable wireless operation with high transition-frequencies ($f_T \geq$ 15GHz) provide the best in terms of noise performance and sufficient amplification.

Having chosen and obtained an appropriate transistor, the next step is to bias the device correctly. If the collector current is insufficient, the transistor cannot provide enough amplification and SNR degrades. On the contrary, a high value for collector current adversely increases the shot noise, again degrading SNR. Therefore an optimum value in between these extremes should be chosen as the collector current.

Finally, it is essential that the transistor must be loaded with an appropriate microwave load at the input port (and its corresponding reflection) [26]. This load point, also called the lowest noise figure point on the Smith Chart, is a characteristic of the transistor, and is highly dependent on the biasing conditions I_C and V_{CE}. Furthermore, it can often be found on the datasheet or S-parameter data of the transistor. Although noise figure data generally lacks low frequency values (less than 100Mhz), it is reasonable to assume that the data for 100Mhz closely match the data for the nearby interval of 10-100Mhz.

Although transistors with high f_T provide a rather high gain for VHF band (30-300Mhz), their maximum stable gain (MSG) is lower to prevent oscillations. Combining lower MSG with higher gain (50+ db) required to suppress noise in the later stages; a two-stage amplifier design is required. Furthermore, possible resistive loading might be needed for interstage stability.

Resistive loading technique is used to improve the stability of multi-stage amplifiers at the expense of gain. Lack of stability, "oscillations", occur when any active 2-port device presents a negative resistance in input or output port, which might possibly result in a reflection coefficient greater than 1 (i.e. $|\Gamma_{in}| > 1$ or $|\Gamma_{out}| > 1$). Adding resistive series loading in between stages is a good way to correct negative resistance and decrease the magnitude of reflection coefficient below 1.

Resistive loading can be helpful in other situations besides increasing stability: Decreasing gain on purpose is one example. Although high gain is required, higher gain may result in other problems, particularly through the saturation of amplifiers. A transistor, when used in an amplifier, acts linearly for low-power input signals. The model predicts that linearity will start to degrade when the input power increases, first by the break of small signal assumptions (soft distortion) and later by the clipping of signal (hard distortion). In a datasheet, the distortion performance of a transistor is defined by intercept points. 1-dB intercept point, defined by the output power in which the nonlinearities decrease the gain by 1 dB over the small-signal gain.

$$G_{1dB}(dB) = G_P(dB) - 1 \tag{3.4}$$

The 1-dB intercept point can be obtained for a specific transistor for a specific bias point. It is highly dependent on the collector current (I_C); however the real P_{1dB} value for a particular I_C can be extrapolated from the given data.

The schematic of the preamplifier is given in Figure 3.7.

3.2.1.1 Parameters and Calculations

There had been two transistor candidates for our design: Motorola MBC13900 (currently Freescale MBC13900) and Infineon BFP420. Both were designed to work on GHz-band and have excellent noise characteristics. Unfortunately their high VHF-band gain made them susceptible to oscillations. Samples for both transistors were obtained and tested and eventually Infineon's BFP420 is chosen

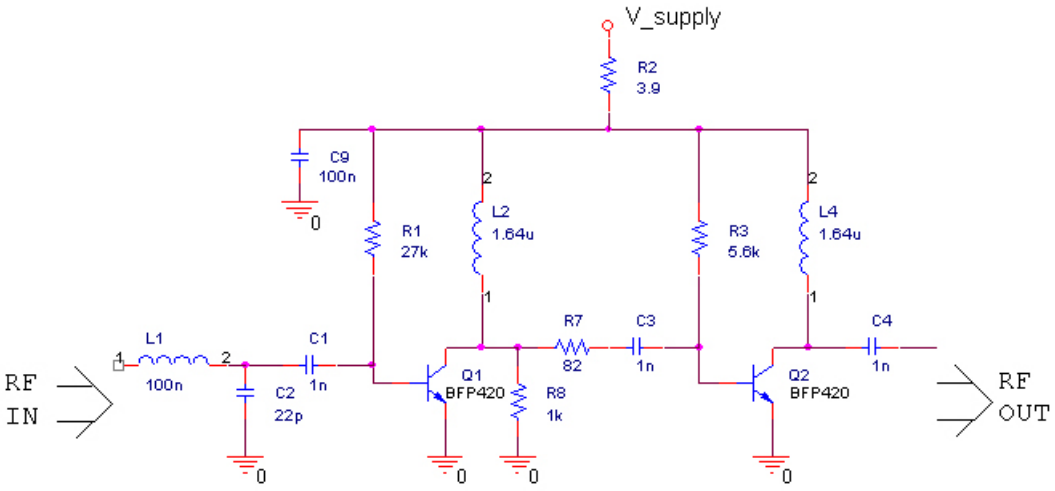

Figure 3.7: Schematics of the preamplifier: The preamplifier consists of two cascaded BFP420 transistors with an low-noise matching circuit in front. The transistors are biased through RF chokes.

for slightly better performance and better commercial availability.

Infineon BFP420 is a NPN Silicon RF transistor in the SEIGET 25 GHz f_T line. It is housed in a SOT323 package and has a nominal DC current gain (h_{FE}) of approximately 100. It has a minimum NF of 0.75dB ($I_C = 2mA$) and a MSG of 36dB ($I_C = 20mA$) for frequencies below 900Mhz. Some S-parameters for 50 and 100Mhz are tabulated below:

f GHz	S11 Mag	S11 Ang	S21 Mag	S21 Ang	S12 Mag	S12 Ang	S22 Mag	S22 Ang
0.050	0.8679	-4.6	9.846	176.3	0.0052	82.4	0.9915	-2.6
0.100	0.8606	-9.4	9.807	173.4	0.0099	84.9	0.9866	-5.1

Table 3.1: S-parameters of BFP420 for $V_{CE} = 1.75V$, $I_C = 5mA$

f GHz	S11 Mag	S11 Ang	S21 Mag	S21 Ang	S12 Mag	S12 Ang	S22 Mag	S22 Ang
0.050	0.5919	-9.3	28.145	173.2	0.0048	79.8	0.9717	-5.2
0.100	0.5876	-19.3	27.744	167.3	0.0081	82.9	0.9577	-10.5

Table 3.2: S-parameters of BFP420 for $V_{CE} = 1.75V$, $I_C = 12mA$

For the DC biasing and RF coupling of transistors, inductors and capacitors

were used frequently. Inductors, acting as RFC, were selected to be the highest nonmagnetic value available, 820nH and were mostly used as pairs. Impedance of a single 820nH at 64Mhz is

$$Z_L = j\omega L = j \cdot 2\pi \cdot 64 \times 10^6 \cdot 820 \times 10^{-9} = 330j\Omega, \tag{3.5}$$

which is sufficiently high to block most of the RF when used in pairs. Similarly, capacitors of value 1nF were chosen for AC coupling purposes and 100nF for stabilization - prevention of undesired feedback and fluctuations. The impedance of 1nF, taking only capacitance into account, is

$$\frac{1}{j\omega C_{1n}} = \frac{1}{j \cdot 2\pi \cdot 64 \times 10^6 \cdot 10^{-9}} = -2.5j\Omega. \tag{3.6}$$

The impedance of 100nF is even lower. Furthermore, for each decoupling capacitor of 100nF, an additional 1nF was placed in parallel. This configuration increases the decoupling efficiency especially at high frequencies.

3.2.2 Laser Diode Circuitry

The laser diode circuitry is the part responsible for the conversion of MR signals from electrical to optical state. It is placed just after the preamplifiers in the RF signal path of the fiber-optic MRI probe.

The reason why this circuit is preceded by preamplifiers is purely noise performance. The electrical-optical-electrical (E-O-E) conversion process, part of which is the laser diode circuitry is inherently associated with a loss in the transmitted power. When combined with the higher noise levels introduced in this section (i.e. intensity and shot noise), this attenuation can lead to fatal results: massive SNR degradation or even the disappearance of signal beneath the noise. Adding preamplifiers prevents this problem, provided that the gain is sufficient enough to move the signal away from the noise floor even after attenuation.

The laser diode circuitry consists of a L-match section, a bias-tee and the laser diode itself:

- The L-match is responsible for the matching of the laser diode to the output of the preamplifier. Using the diode model generated through small-signal approximation [27], it can be predicted that the laser diode would have an RF resistance in between 4Ω (with an ideality factor of $n = 2$) and 6Ω ($n = 3$). Since the output impedance of BFP420 is very high compared to this resistance, the L-match ensures efficient coupling of power from the amplifiers to the laser through the bias-tee.

- Bias-tee is a simple T-shaped circuit used to mix or separate RF and DC into / out of a single microwave port. It is made of a single capacitor at the left arm of the *T-topology* becoming the RF port and an inductor on the right arm as DC port. The remaining port (RF&DC) is the tapping in between the capacitor and inductor and it is where the laser diode is connected. During operation, the power supply circuitry drives the laser diode by injecting current through the DC port, and the RF port efficiently transmits the MR signals to the laser diode with the help of L-match.

- The laser diode is connected to the RF&DC port of the bias-tee on one side and to the fiber-optic cabling on the other. It is in the core of electrical-to-optical conversion process, and the part holding the micro-lens to couple the generated optical energy to the fiber.

Finding an appropriate laser diode had been significantly harder than finding a transistor. Unlike transistors, semiconductor lasers are expensive devices with higher costs of production which limited their spectrum. Furthermore, a low-noise laser with low power and small size characteristics is even more uncommon. Applied Optoelectronics Inc.(Sugar Land, TX) has been a manufacturer of low-noise lasers; and they have agreed to house some of their lowest-noise lasers in a coaxial package for our use. This custom made laser turned out to be a good choice, due to its specific properties of central wavelength, responsivity, optical power, threshold current and RIN value.

Wavelength: Unlike Wavelength Division Multiplexing networks or other optical applications, the frequency and wavelength of the diode was not important in this application. In fact, the choice of wavelength was determined by other more

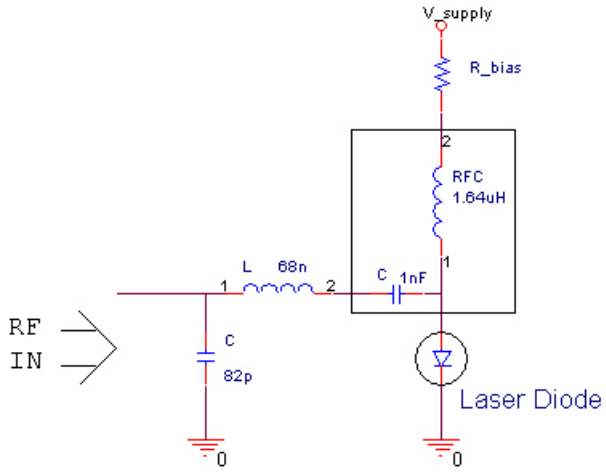

Figure 3.8: Schematics of the laser diode and relevant circuitry: The power matching circuit is followed by a bias-tee in the middle of which is the laser diode.

important factors, such as fiber dispersion and attenuation: The two minimas of fiber dispersion and attenuation are located at $\lambda = 1.3\mu$m and $\lambda = 1.55\mu$m; and among the lasers with low RIN values, 1.55μm ones are the less noisy lasers.

Responsivity: Responsivity Γ is defined as the differential change in output power per differential change in current through the laser diode,

$$\Gamma = \frac{\partial P_0}{\partial I_d}. \tag{3.7}$$

Responsivity is directly linked with the loss associated with E-O-E conversion. However the variance of responsivity values over different brands and models of low noise lasers (1.3μm and 1.55μm) was extremely low: every single one had a responsivity in the range 0.12-0.15W/A.

Optical Power: Although there was no explicit constraint on power, there were advantages of having a low powered laser diode: First, lower power generally implies lower threshold current which was extremely desirable. Second, higher powered diodes tended to have higher RIN values and higher RIN values meant they were considerably more noisy.

Threshold current: Since the P_0 vs. I_d plot was pretty linear, any DC bias current level greater than the threshold current would have yielded the given

responsivity in the design. Taking into account the low-power requirement and the fact that lower operating currents created lower laser intensity noise, it became reasonable to use a low threshold laser.

Relative Intensity Noise: In the datasheet of a communication laser, almost always the Relative Intensity Noise value is specified. However, care must be taken: This value is "relative", it is normalized over its optical operating power. The absolute data to be compared among lasers is the *intensity noise power*, which can be calculated using the value of optical power and RIN. The lasers with lowest noise power must be chosen.

Fiber Connector: For our purposes, a pigtailed laser proved to be useful. Since it has a built-in fiber, there was no need to couple the laser to fiber. Also, a pigtailed laser had a connector on the other end, which permitted easy linking to the photodetector. In the actual design, a SC/APC connector was used. SC connectors present a lower Insertion Loss (i.e. the loss generated due to the connector) and they have better resistance against the possible damage on fiber caused by mechanical stress. Moreover, the APC suffix on the connector means "Angled Physical Contact" polish, in which the end of fiber is not perfectly perpendicular to the fiber, but has a slightly round ("physical") shape with 8 angle ("angled"). Using an APC polish results in a lower back-reflection rate, although it is harder to align an angled fiber. In our case, lower back-reflection rate was highly desired, since any external reflection back to laser led to an increase in laser intensity noise.

Temperature and Cooling: Although it is common the laser diodes with butterfly packages to come with Thermo-Electric Coolers (TECs), they are generally avoided in coaxial housings for a couple of reasons. First, they are needed to eliminate any temperature related effects on wavelength and stabilize it. Since the fiber-optic MR probe was insensitive to the value of wavelength; the drift of wavelength over temperature or time could be allowed. Also, the laser diode was not operated at maximum power and measurements indicate that the heat generated was not high enough to require TEC. Last but not the least, TECs are essentially peltier devices and they tend to draw a lot of current (in the order of

amperes) which did not comply with the power specifications. But it should be noted that using the diode without cooling has some adverse effects like shortening the lifetime of diode - turning off the cooler is used in accelerated-aging tests with operation at maximum power.

Package: For fiber pigtailed lasers, two common types of packaging are used: butterfly and coaxial. Butterfly case, mostly used in high-power or stable-wavelength laser applications, is the bigger among the two and is shaped as a rectangular prism. Its larger volume enables it to house thermal monitoring devices (thermistors) and thermoelectric coolers together with the optical devices: laser, micro-lens for coupling and monitor diodes for continuous measurement of output power. Coaxial package, which only contains the optical devices, is substantially smaller with its cylindrical shape of diameter 5.6mm. Naturally, the coaxial package was far more suitable for out purposes.

One last remark about the package is related to the optical components it contain: In low-noise lasers, reflections must be avoided as much as possible; as they increase the noise level. One way of reducing reflections is to use an APC connector with angled reflections. Another common way is to use optical isolators which are not MRI-compatible since they rely on the Faraday Effect to work.

An optical isolator consists of two polarizers, one of which is rotated 45° relative to the other, and a Faraday rotator in between them. The Faraday rotator is responsible for the 45° rotation of the polarization of incoming laser beam; which enable the forward traveling beam to pass through both polarizers unblocked. However the Faraday rotator is not reciprocal: if the reflections (i.e. reverse-traveling beam) pass the second polarizer they experience the same rotation again, becoming totally perpendicular ($45° + 45° = 90°$) to the first polarizer that blocks.

Unfortunately Faraday Effect depends on the magnetic field parallel to the direction of propagation, dictated by

$$\rho = VB, \tag{3.8}$$

where ρ is the rotary power (angle per unit length), B is the parallel magnetic

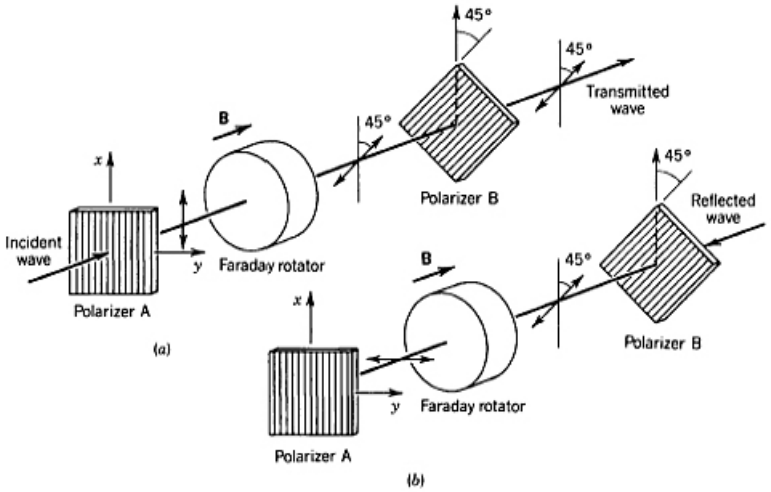

Figure 3.9: Inside an optical isolator: (a) it transmits light in one direction, correctly rotating the polarization and (b) blocks in the other direction by excessive rotation. Property of B.E.A. Saleh and M.C. Teich [20]

flux density, V is the *Verdet* constant. For a constant 45° rotation, the length and B field must be adjusted; and powerful external fields such as the fields in Magnetic Resonance Imaging severely distort this adjustment, changing the rotary power to an arbitrary value. Also note that there is a risk of permanent misplacement of the isolator with the effect of external field, blocking the signal path completely, which is another reason to eliminate optical isolators from the design at the expense of increased noise.

3.2.2.1 Parameters

The laser was manufactured by Applied Optoelectronics Inc. with part number DFB-1550-C5-2-A-SA-A-A-02, housed in a coaxial package. It was a Multi-Quantum-Well (MQW) Distributed Feedback (DFB) laser designed for analog modulation in Cable-Tv return path applications and it was fitted with a SC connector having *Angular Physical Contact* polish.

Its central wavelength is 1.55μm with an optical power of 2mW at the operating current 30mA. The threshold current is 12-13mA depending on the particular sample and the responsivity is around 0.12-0.13W/A. The Relative Intensity

Noise range from -153dB/Hz to -155dB/Hz, both of which are very low values.

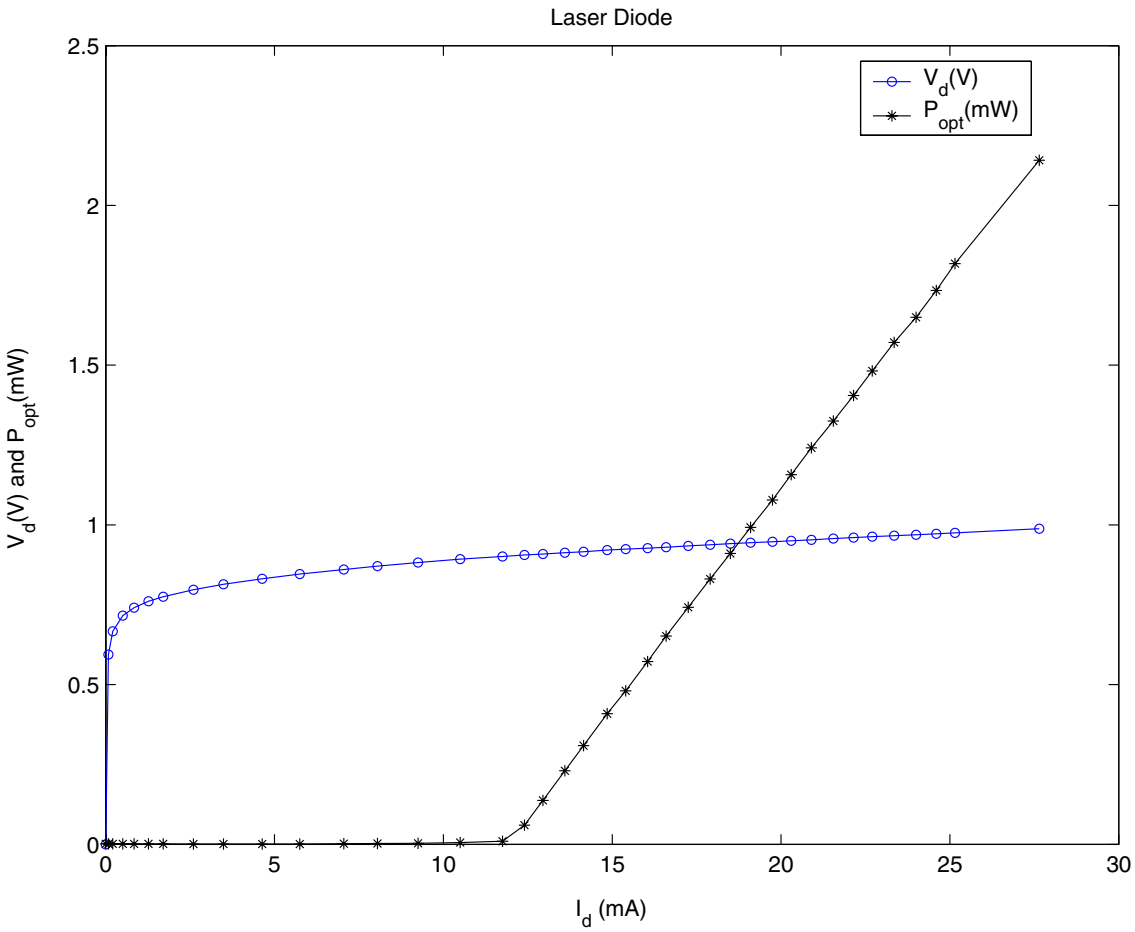

Figure 3.10: P_{opt} and V_d vs. I_d plot of the laser diode: Note that beyond threshold current, the power vs. current linearity of the laser is excellent.

Although the laser was custom built based on our decisions, eventually modification on the lasers was needed: Removal of the optical isolator and realignment of the fiber were done in our optic labs using a XY-translation stage ([ν]-9064 from New Focus, San Jose, CA), Z-translation stage (Model-440 from NewPort, Irvine, CA), a rotational stage (Model-485 from NewPort) and dual fiber alignment stages (F-915 from NewPort). The power measurement during realignment was done using a handheld power meter from New Focus (Optical Power Meter Model-840 with 818-IR Head). A metal epoxy was used for the fixation of fiber and diode modules.

The bias-tee of the laser diode consisted of dual 820nH inductors yielding 1.64μH in total, and a coupling capacitor of 1nF.

3.2.3 Power and Control Circuitry

The power and control circuitry is responsible for supplying power to the rest of the transmitter and switching it when necessary. This section is designed not to contain any RF power and it not a part of the signal path.

This circuit includes another fiber-optic line (control fiber) connected to a photodetector diode (PD): A photodetector diode is a device which acts like an optically controlled current source. In fact, it is a reverse biased diode in which reverse saturation current is optically controlled. The light falling onto the diode creates optically generated EHP which add up to the minority carrier density and get swept to the other side of the diode becoming the reverse saturation current.

Regarding the operation of PD, when there is no light shining on the photodetector, the whole circuit becomes completely off; except a very little amount of current leaking through the photodetector - called the dark current. This current is on the order of tens of nanoamperes; therefore the power consumption in OFF state is extremely low.

The diode is connected to a PNP transistor in a Darlington configuration. When an external source activates photodetector, it acts like a current source and conducts a known amount of current, which generates a voltage greater than the base-emitter on voltage ($V_{BE(ON)}$) of the PNP transistor. Dictated by Kirchoff's Laws, the current flowing through the resistance R_{switch} is only part of the current conducted by the diode, the rest of which becomes the base current of the transistor. This base current is adjusted to be sufficient enough to put the transistor into saturation, providing $\sim$2.9V to the rest of the device, including amplifiers and laser diode.

A more sophisticated design adds another state to the device besides on and off. The third state is initiated by shining even more light to the diode and can

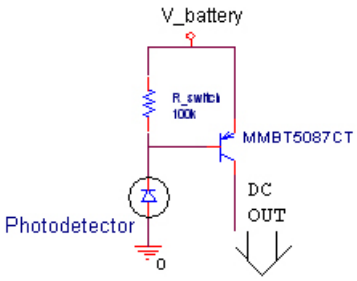

Figure 3.11: Simple power circuitry: Drawing sufficient current from the photodetector makes the PNP transistor go into saturation; yielding 2.9V to the rest of the circuit.

be used for active decoupling purposes. In this configuration, the cathode of the photodetector is connected to a PIN diode with a shunt resistor R_{shunt} instead of ground. During the activation of diode with low-intensity light, the PIN diode stays inactive with all current passing through R_{shunt}. However, high-intensity light generates more current, enough to induce voltage more than $V_\gamma + V_{BE(ON)}$ on the shunt resistor to simultaneously turn the NPN transistor and PIN diode on. Thus, control of the circuitry and the active decoupling can be realized semi-separately with a single fiber line.

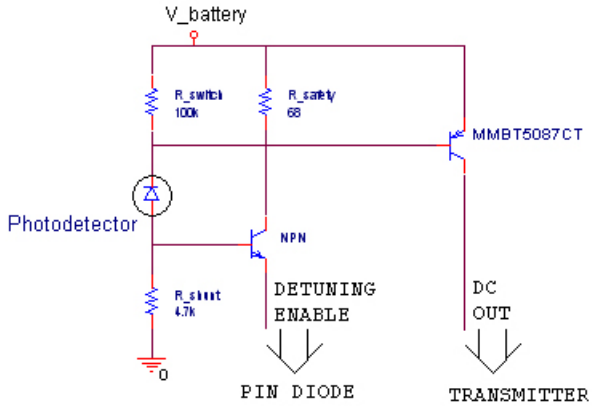

Figure 3.12: 3-state power circuitry: Increasing the light falling onto the photodetector triggers the PNP transistor which switches the rest of the circuit. Further intensification of the light also puts NPN transistor into ACT state - turning on the active tuning.

3.2.3.1 Parameters

In the core of the system was the photodiode: Manufactured by Industrial Fiber Optics Inc., the diode IF-D91 is a high speed, low-cost photodetector in a plastic housing. It is sensitive to a wavelength range from 400nm to 1100nm with a peak responsivity of $0.4\mu A/\mu W$ around 880nm. It is connected to a Light Emitting Diode(LED) operating at 870nm matching the peak responsivity. The connection is through a 1000μm multi-mode(MM) fiber (SH4001, I. Fiber Optics, Inc.).

The PNP transistor in Darlington configuration was Fairchild MMBT5087CT. It is a general purpose amplifier with a minimum DC gain(h_{FE}) of 250. Its high gain and low collector-emitter saturation voltage ($V_{CE(sat)}$: maximum 0.3V, measured 0.1V) made it a great transistor for switching the transmitter on and off.

NPN transistor was only used as a current amplifier, therefore its characteristics was not important; the only requirement was to have a DC current gain sufficiently high to supply 10mA to the PIN diode.

3.2.3.2 Calculations

R_{switch}: This resistor is responsible for the switching of PNP transistor. Therefore choosing a low value would require more current passing through R_{switch} which would make the circuitry inefficient and less practical. On the contrary, a high value would somewhat limit the saturation of transistor by decreasing the base current, and it would also slow down the switching of the transistor from on to off. Between these boundaries, 100kΩ turned to be a suitable and standard value.

$$R_{switch} = 100k\Omega. \tag{3.9}$$

R_{shunt}: The reason a shunt resistor is added in parallel to the PIN diode is to limit the PIN diodes operation when the amplifiers and coil need to be active. Therefore, this resistor should be small enough to generate a voltage lower than $V_\gamma + V_{BE(ON)}$. However, it should also be high enough to activate the NPN

transistor to let ∼10mA current pass through PIN diodes when high-intensity light is shined on the photodetector.

$$R_{shunt} \cdot I_{PD,low} < V_{\gamma} + V_{BE(ON)}, \tag{3.10}$$

$$R_{shunt} < 6k\Omega. \tag{3.11}$$

Looking at the more strict requirement of supplying 10mA current to active detuning, the selected value was 4.7kΩ,

$$R_{shunt} = 4.7k\Omega. \tag{3.12}$$

R_{safety}: Acting as the safety resistor, R_{safety} is to limit the maximum current through the PIN diode if, for some reason, an error such as short-circuit occurs. Its value was chosen low enough not to affect the operation of the rest of the circuit,

$$R_{safety} = 68\Omega. \tag{3.13}$$

3.2.4 Complete Schematics of the Transmitter

Having explained the parts, it would be true to say that the whole system was more than the parts combined: Although each section was defined, there were more than one way to combine them. Thus, there were two different schematics for the transmitter: high voltage - low current design and low voltage - high current design; and as in all designs there was a tradeoff.

The reason why low current would be more preferable against the high, lied primarily in how the power would be supplied. Battery supplied power always have had limits which were not explicitly stated in the datasheet, one of them being the internal resistance. Internal resistance of a cell is the physical limit on the maximum current it can supply. Therefore, even though a battery is rated 25mAh, it might not give 20mA at all. This was a very solid reason to design circuitries working with high voltage and low current ratings.

The problems with using high voltage low current designs were the increased risk of oscillations due to the extra feedback and the increased switching time. High voltage designs usually fed the biasing current through more than one active device on the signal path, i.e. transistor, laser diode. Moreover, they used RFC to route the RF signal correctly. However, RFC are not perfect, they pass a very small part of the RF power, which would result in a feedback that may result in oscillations in such a high-gain system. As a second point, RFC are inductor based components: Combining the slowness of RFC with the EHP generation and destruction processes in semiconductors, the switching time of the transmitter dramatically increased.

Considering the tradeoff between two different design approaches, we created two different circuits, one working with 1.5V and the other at 3V. Although they have had different DC equivalent circuits, RF signal path was the same for both designs.

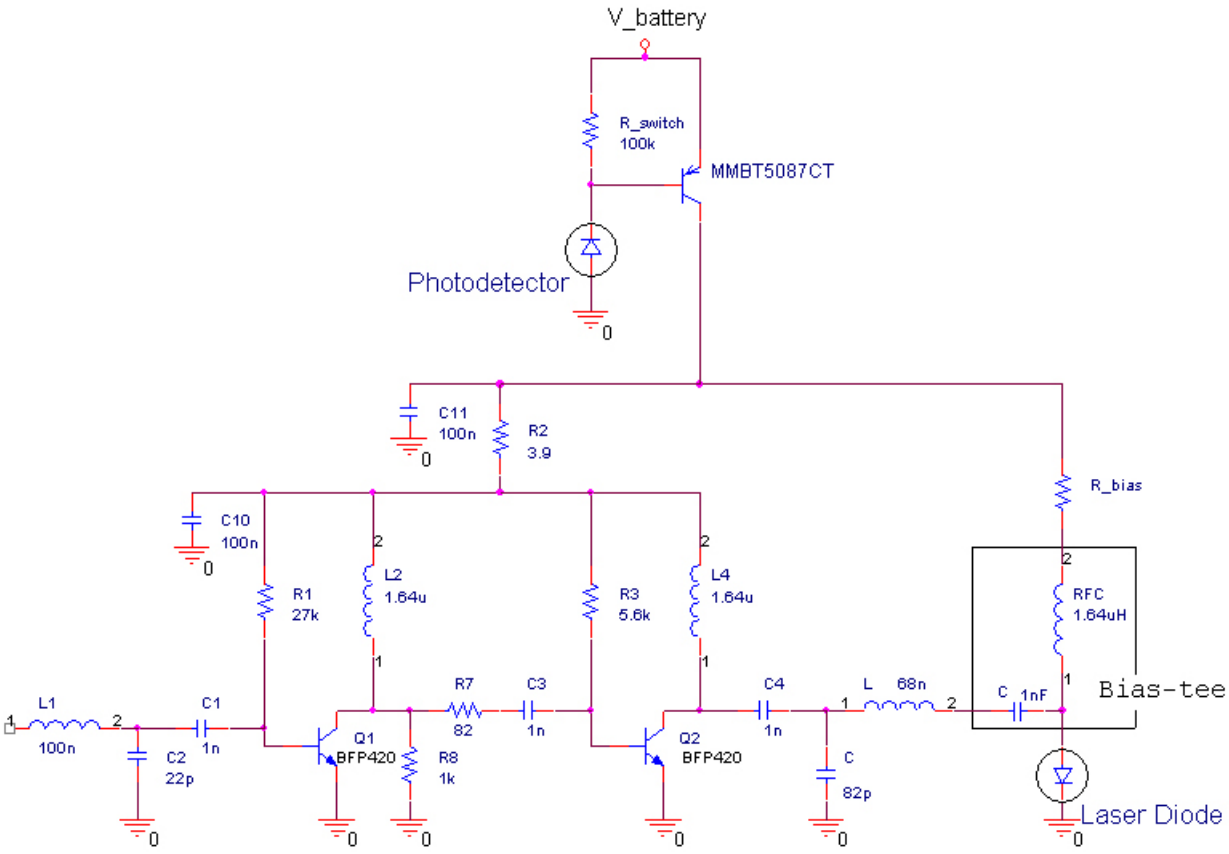

Figure 3.13: Overall schematics for 1.5V design: The preamplifiers and laser have their own biasing circuitries.

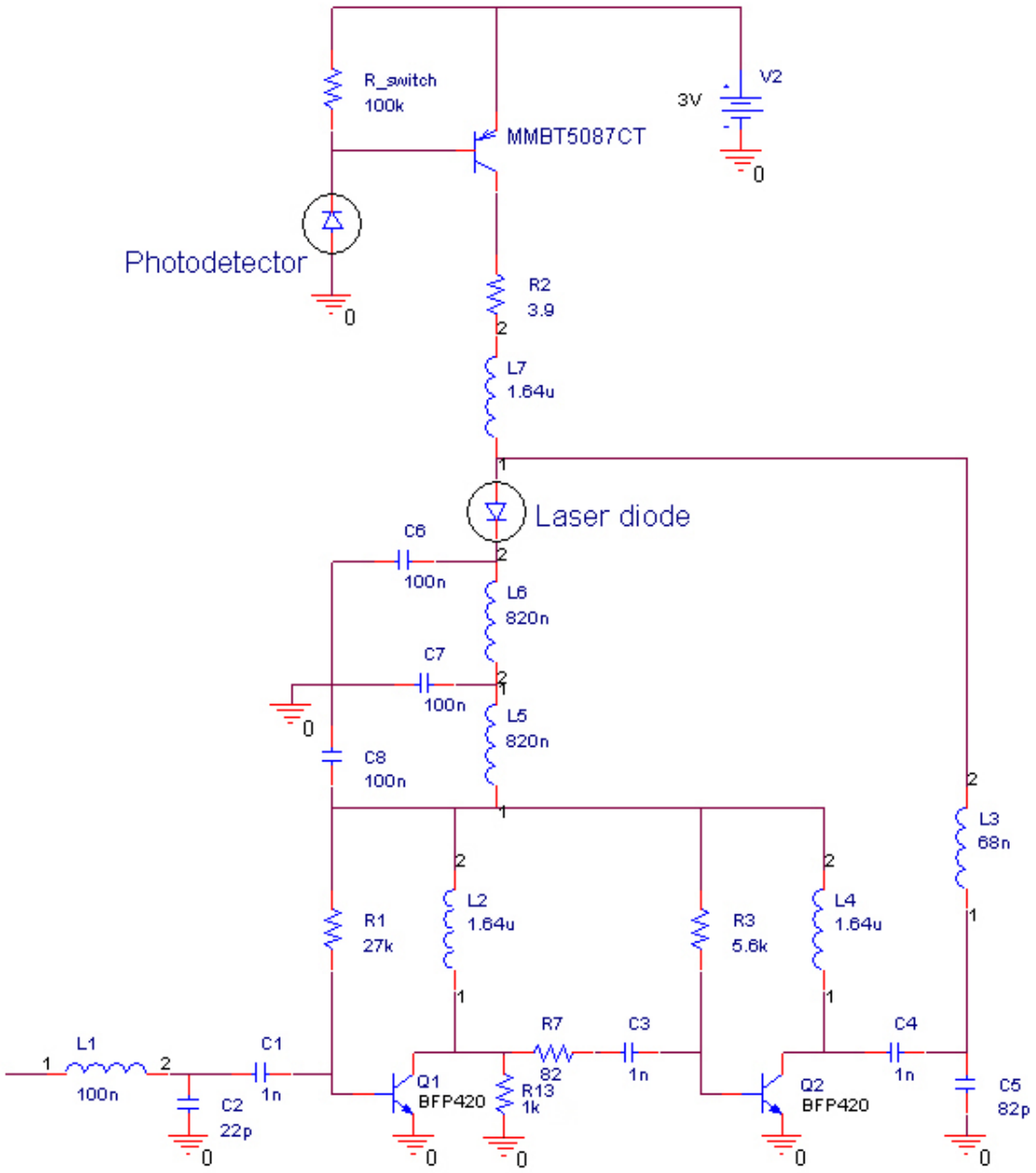

Figure 3.14: Overall schematics for 3V design: The same current biases both the laser and the preamplifier.

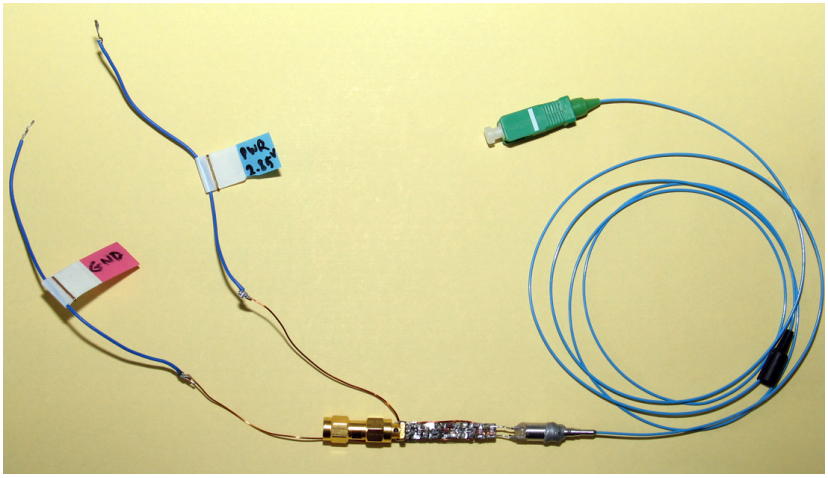

Figure 3.15: Photograph of the transmitter with modified laser

3.3 Receiver and External Control Circuitry

The receiver and external control circuitry is the part connected to the MRI scanner. It is a rather small section with simple circuits with their own power supply. The optical fiber constitutes the receiver's only connection to the transmitter and coil.

3.3.1 Receiver

The MRI signals, after being coupled to the optical beam in the fiber are then transmitted to the receiver. The main responsibility of the receiver is to convert optical signals back to electricity, and it uses a special photodetector.

Analyzing the laser beam that falls on the PD, it can be observed that the envelope of the beam consists of two components, the one generated by MRI signals and the one generated by the DC biasing current of the laser diode. The current that photodetector generates is actually the sum of these components converted. As the demodulation of the optical carrier is done internally by the photodetector, the only circuitry needed is a bias-tee to separate these two components.

The bias-tee circuitry, which is used at the output of photodetector is responsible for the separation of biasing current and MRI signals, similar to its usage in the transmitter for combining purposes. It has again 3 ports, RF&DC, RF and DC: In our setup RF&DC port is connected to photodetector, DC port to a resistor and RF port becomes the output of the overall design. The MRI signals are passed to the signal processing elements of MRI machines through this port.

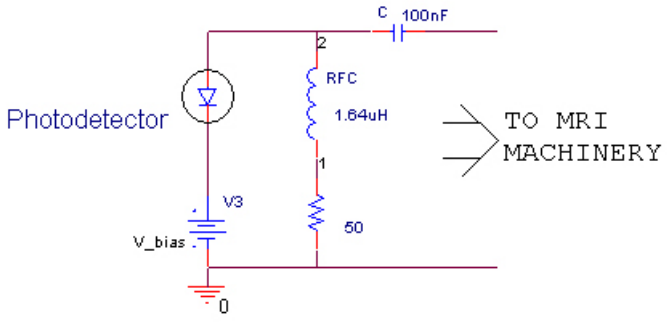

Figure 3.16: Schematics of the receiver: The photodetector converts the optical energy into electrical signals. Then, the bias-tee separates the DC component of the signal from the RF component.

3.3.1.1 Parameters

The photodetector used in this part was a special diode: ETX100RSC-DM, manufactured by JDS Uniphase, West Tranton, NJ.

ETX100 is a 100μm diameter InGaAs photodetector in a plastic housing with a SC receptacle. It has a peak responsivity (minimum Γ_{PD}=0.7A/W, measured Γ_{PD}=0.8A/W) at 1550nm matching the wavelength of the laser. The photodetector has 2GHz bandwidth.

Together with the laser, the E-O-E conversion system showed an attenuation of 19.6dB.

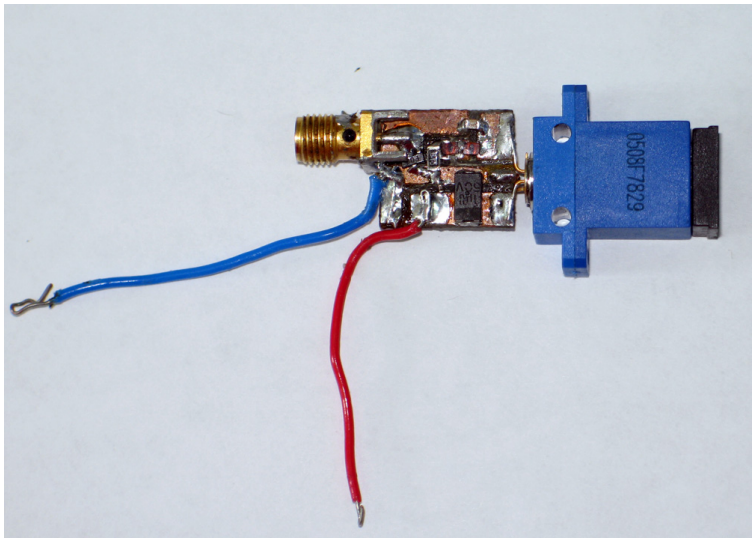

Figure 3.17: Photograph of the receiver

3.3.2 External Control Circuitry

The external control circuitry is the complement of the power and control circuitry of the transmitter.

It simply consists of a fiber pigtailed LED (IF-E91D, 100Mbps IR LED by Industrial Fiber Optics, Inc.) and corresponding biasing resistors. The LED was selected to mate perfectly with the 1000μm fiber. The circuitry has an switch for the overall switching of the transmitter. Also, an input may be needed to switch active detuning if the 3-state control circuitry was used in the transmitter. In each case, the resistor values were chosen to emit the required amount of light to the control fiber with the specific supply.

Note that the switching of the transmitter required 280μW of power through the control fiber, whereas the switching of active detuning required 400μW.

(a) Simple External Control Circuitry (b) Switching External Control Circuitry

Figure 3.18: Schematics of the external control circuitry: It consists of a single LED source with appropriate biasing.

3.4 Noise Calculations

Knowing the sources of noise together with the parts of the prototype and their corresponding parameters, noise calculations of the overall design could be performed. First, the noise powers per Hz need to be calculated with the equations given in Chapter 2,

$$P_{LIN,laser} = 10^{RIN/10} I_{LD}^2 R_L, \tag{3.14}$$
$$= 6.42 \times 10^{-17} mW/Hz \tag{3.15}$$

$$P_{Shot,laser} = 2eR_L I_{LD} \tag{3.16}$$
$$= 2.88 \times 10^{-16} mW/Hz \tag{3.17}$$

$$P_{Shot,PD} = 2eR_L I_{PD} \tag{3.18}$$
$$= 2.56 \times 10^{-17} mW/Hz \tag{3.19}$$

and using these powers, corresponding noise factors were

$$F_{LIN,laser} = 16.11 \tag{3.20}$$
$$F_{Shot,laser} = 72.43 \tag{3.21}$$
$$F_{laser} = F_{Shot,laser} + F_{LIN,laser} = 88.54 \tag{3.22}$$
$$F_{Shot,PD} = 6.44 \tag{3.23}$$

where the noise factor of laser, F_{laser}, was the sum of the contributions from intensity noise and shot noise. Also note that the noise figure of the preamplifier was designed to be

$$NF_{preamp} = 0.88dB. \tag{3.24}$$

The gain of each section

$$A_{preamp} = 50dB, \tag{3.25}$$

$$A_{LD-PD} = \Gamma_{LD}^2 \Gamma_{PD}^2 = 0.0108 = -19.6dB \tag{3.26}$$

was also important in the calculation of overall noise figure, since

$$F_{total} = F_{preamp} + \frac{F_{laser} - 1}{A_{preamp}} + \frac{F_{PD} - 1}{A_{preamp}\, A_{LD-PD}}. \tag{3.27}$$

Combining the calculated values with Equation 3.27, we got

$$F_{total} = 1.23, \tag{3.28}$$

which concluded that the noise figure of the system should be

$$NF_{total} = 0.898, \tag{3.29}$$

which was lower that required limit of 1 dB.

Chapter 4

Simulation Results

Before the prototype was built, simulations had been performed to check the device for any potential problems that may arise. Moreover, simulations helped the construction and debugging process by providing approximate values for the correct measurements. The programs used throughout the process were *Ansoft Designer SE 1.0* by Ansoft Corp. and *Orcad Pspice 9.2.3* by Cadence Design Systems Inc. Additional calculations were done in the environment of *Matlab Release 13* by the Mathworks Inc.

In order, the results of the following simulations are presented here: DC biasing (Figure 4.1), Transient response (Figure 4.2), AC sweep (Figure 4.3) in Pspice and Gain (Figure 4.4), Stability (Figure 4.5), Noise Figure (Figure 4.6), Input and Output impedances (Figures 4.7 and 4.8) in Ansoft Designer.

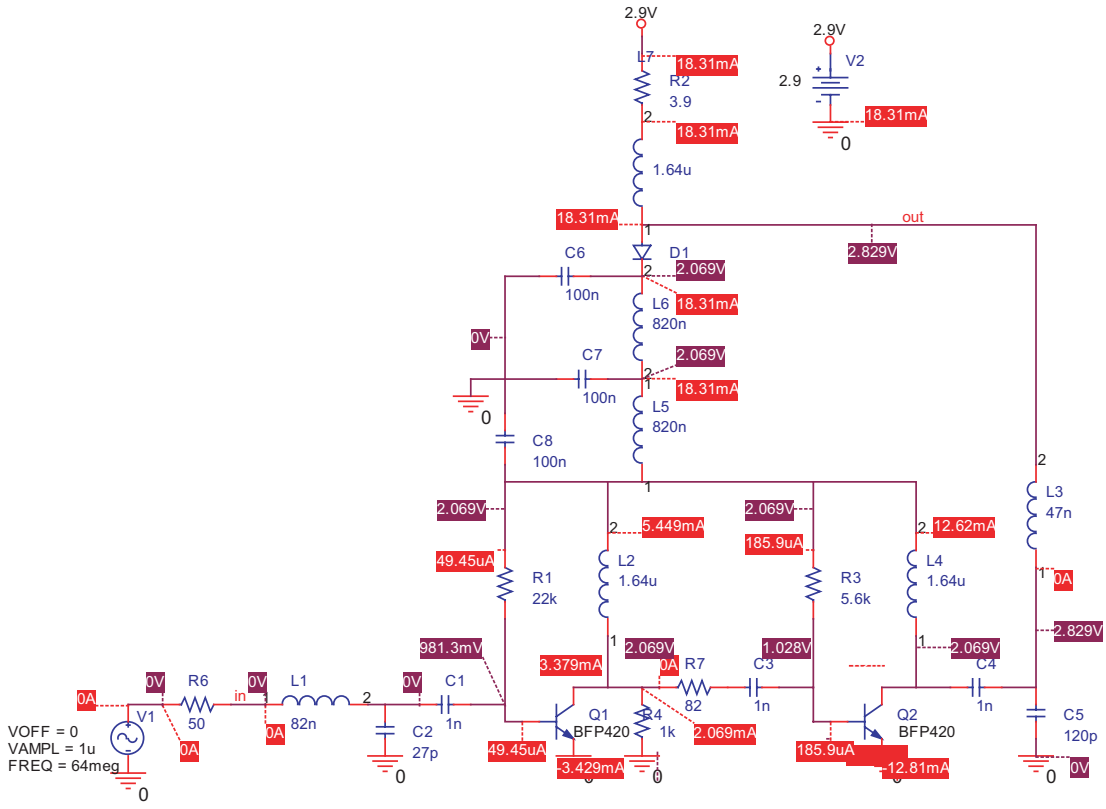

Figure 4.1: DC biasing by PSpice.

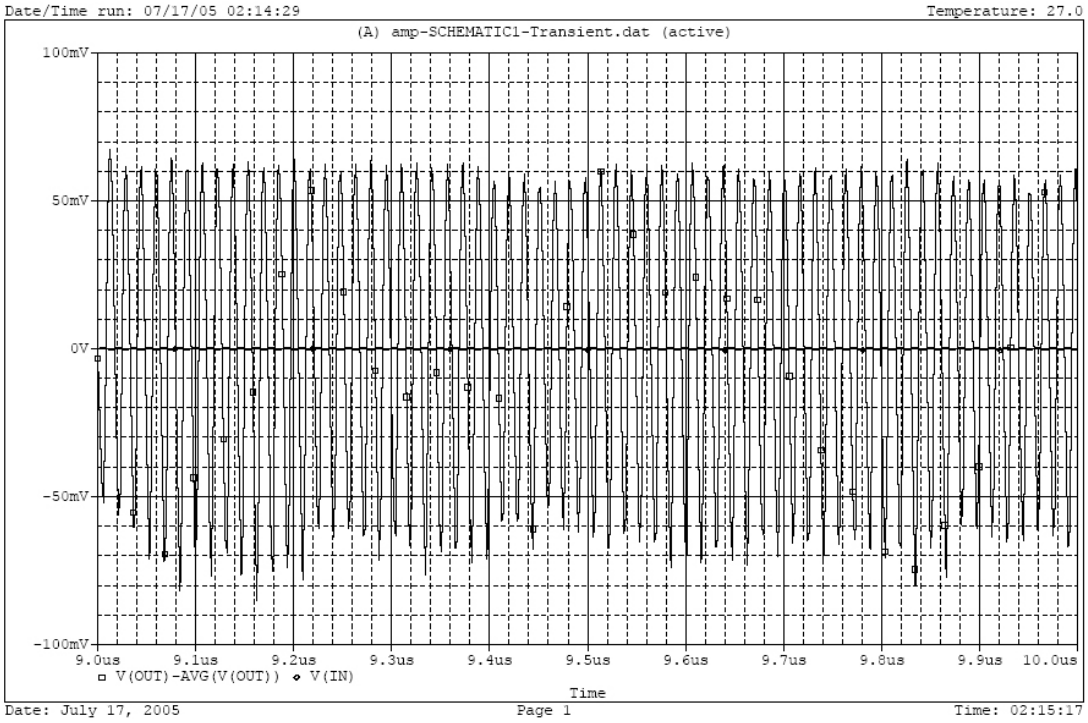

Figure 4.2: Transient response by PSpice: The gain of the amplifier can be deducted from the amplitudes of corresponding signals.

Figure 4.3: AC Sweep by PSpice: Presents the gain of the circuit up to $6Ghz$.

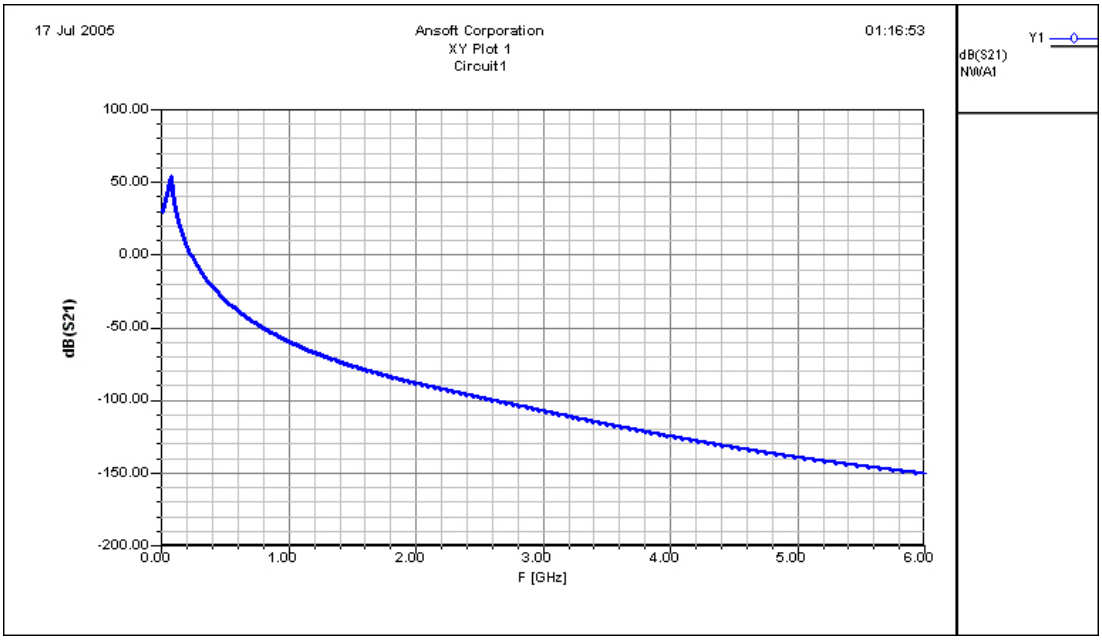

(a) Ansoft Gain simulation from 10Mhz to 6Ghz

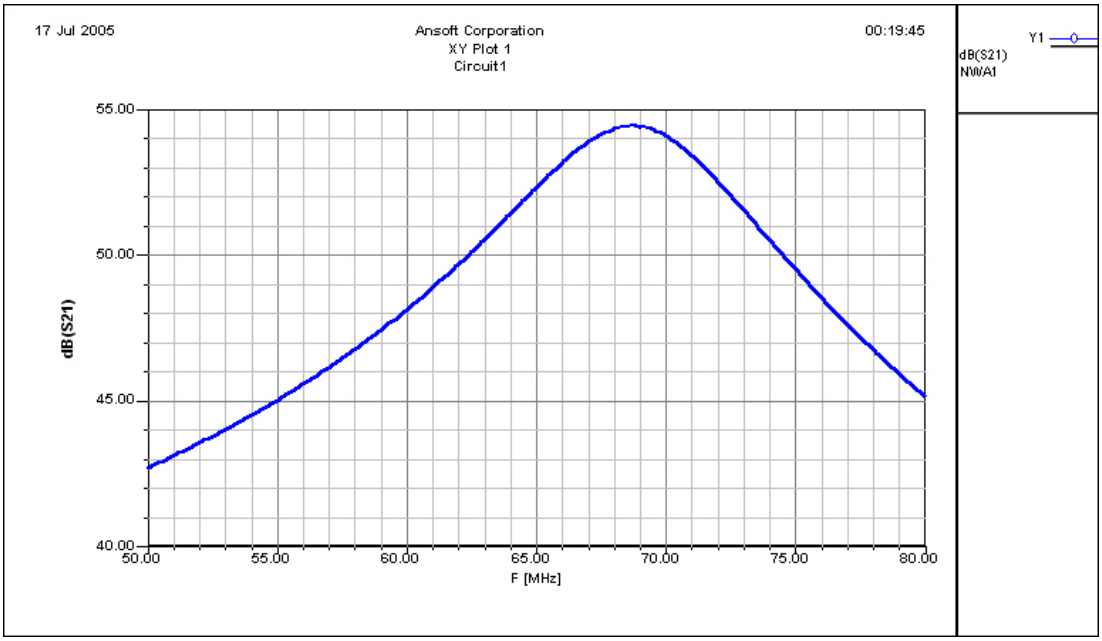

(b) Zoomed to frequency range 50Mhz to 80Mhz

Figure 4.4: S21 - Gain by Ansoft: Shows the gain of the circuit up to $6Ghz$, note that this simulation is more accurate than the one by PSpice.

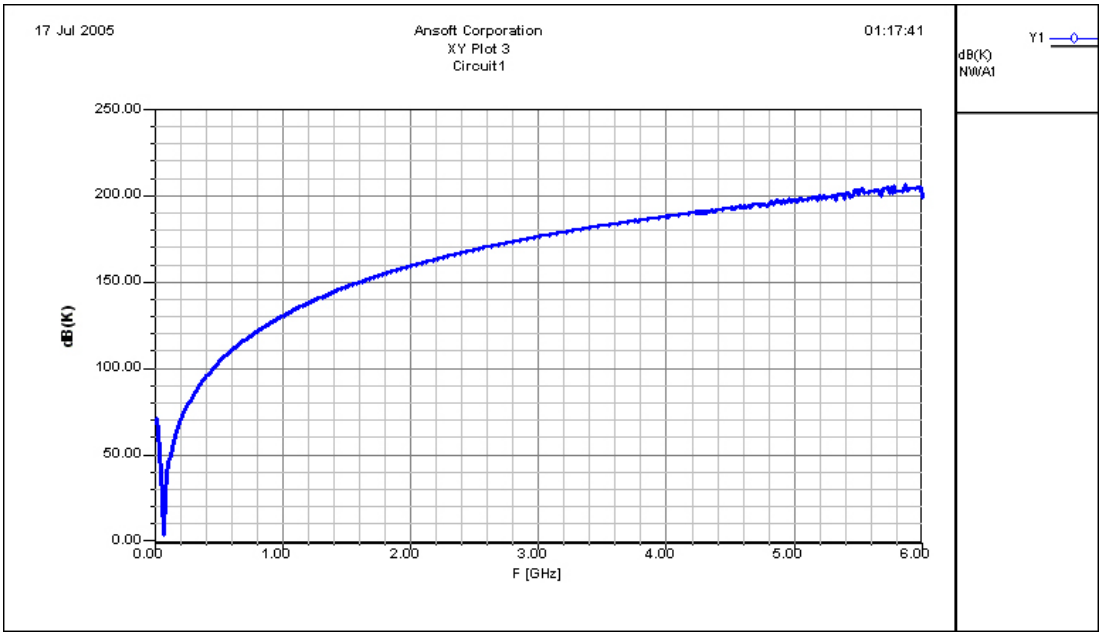

(a) Ansoft stability simulation from 10Mhz to 6Ghz

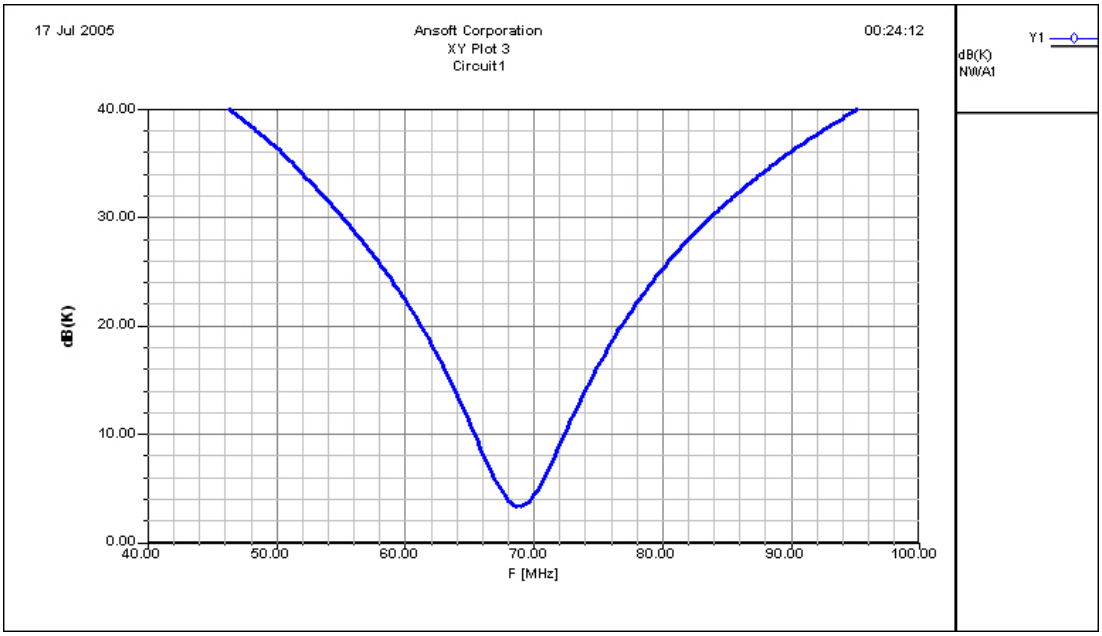

(b) Zoomed to frequency range 40Mhz to 100Mhz

Figure 4.5: K - Stability by Ansoft: The parameter K should be greater than $1dB$ for unconditional stability.

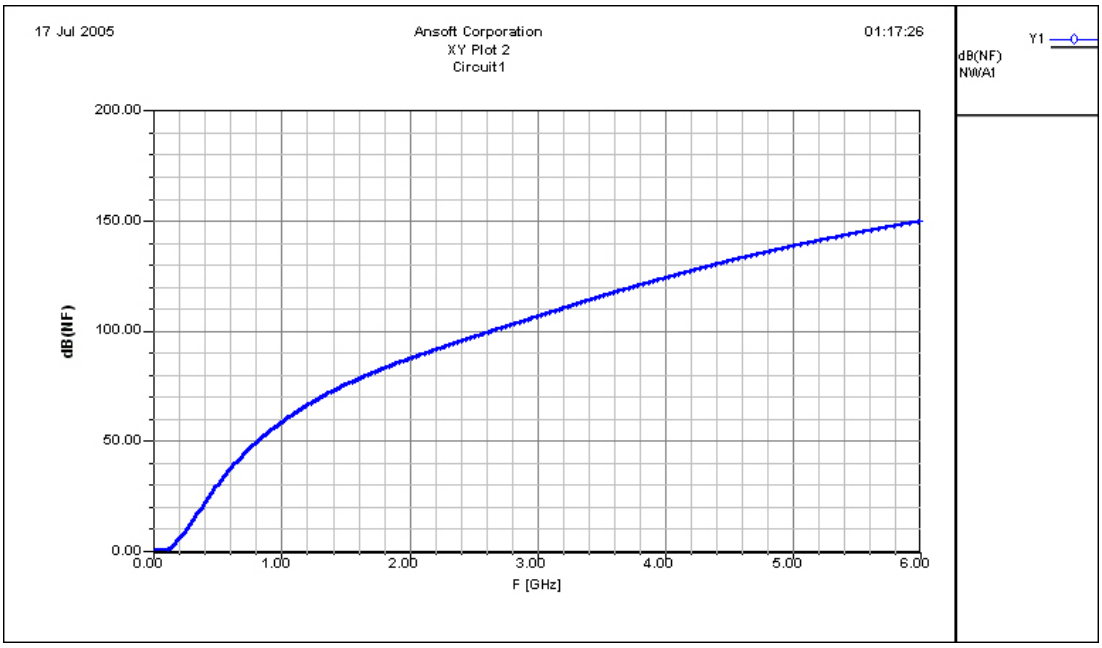

(a) Ansoft Noise Figure simulation from 10Mhz to 6Ghz

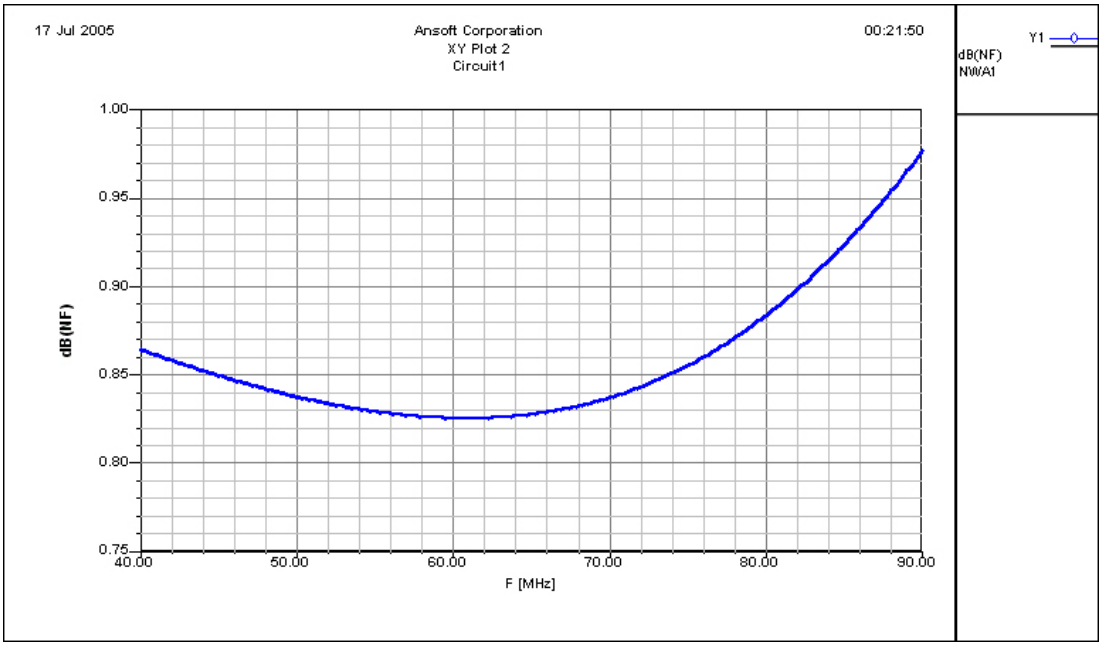

(b) Zoomed to frequency range 40Mhz to 90Mhz

Figure 4.6: Noise Figure by Ansoft: This simulation shows the noise figure of the device versus frequency.

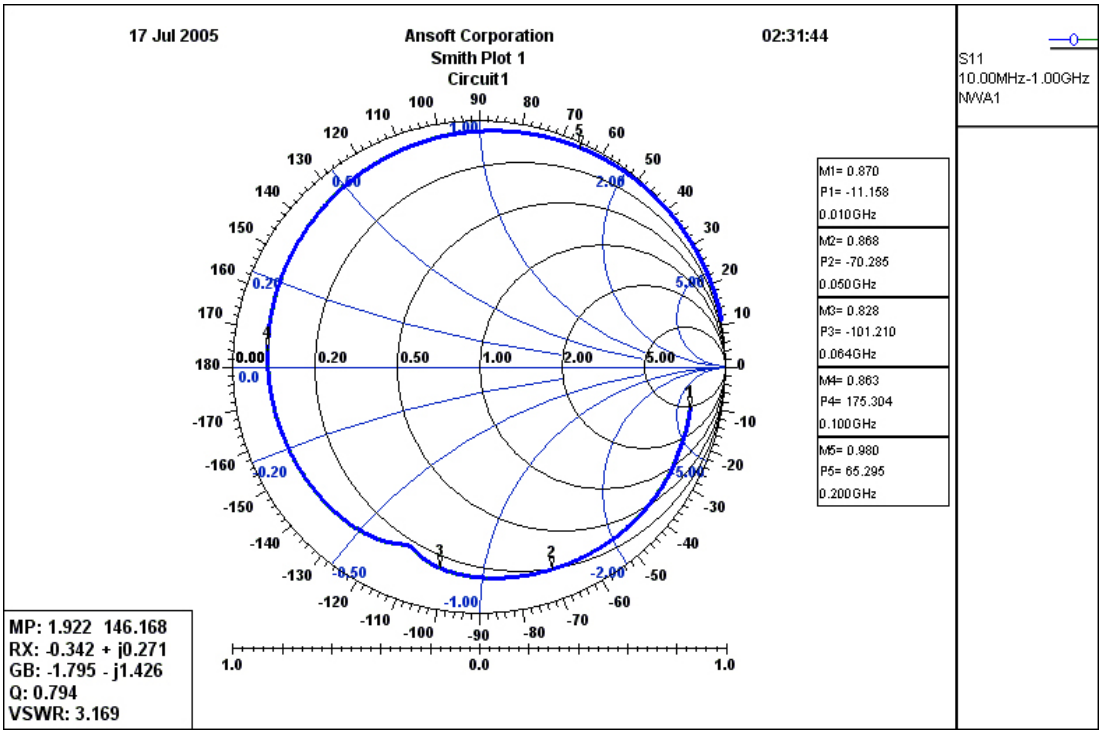

(a) S11 simulation from 10Mhz to 6Ghz

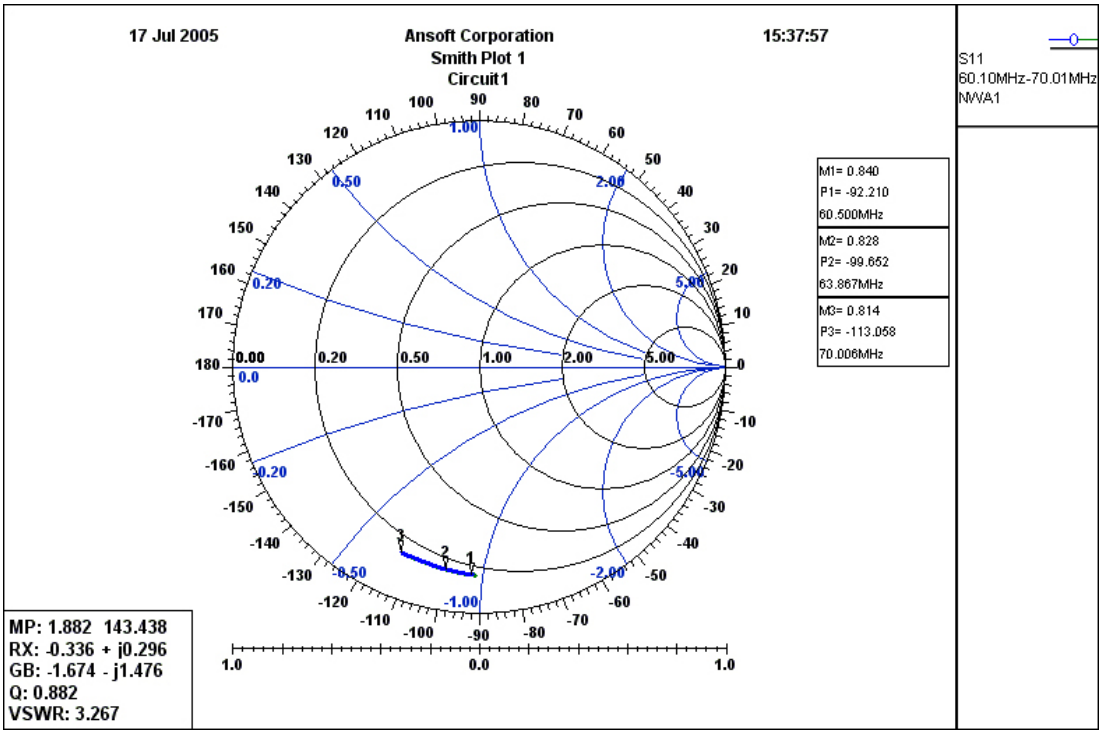

(b) Zoomed to frequency range 60Mhz to 70Mhz

Figure 4.7: S11 - Input Reflection by Ansoft: The input reflection is related to the transistor's input impedance and the matching circuit in front.

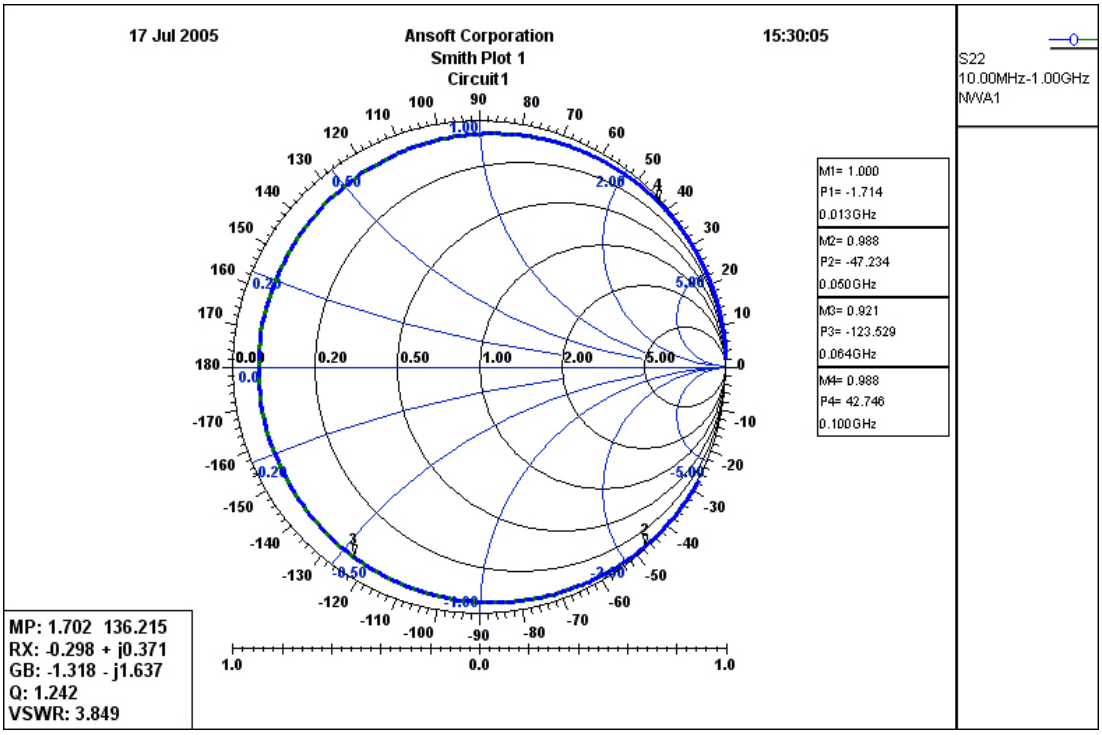

(a) S22 simulation from 10Mhz to 6Ghz

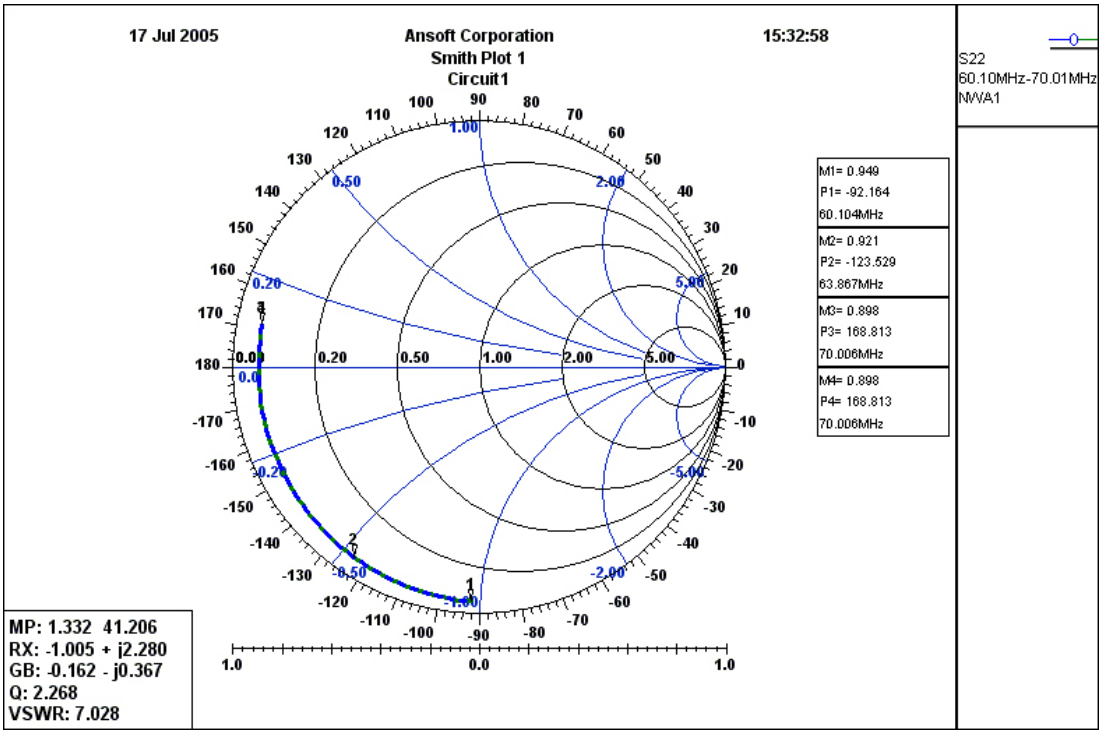

(b) Zoomed to frequency range 60Mhz to 70Mhz

Figure 4.8: S22 - Output Reflection by Ansoft: This is the output reflection observed by the laser diode.

Chapter 5

Experimental Results

The experimental results we have obtained can be divided into two categories, offline measurements and online measurements. Offline ones correspond to the experiments using laboratory equipment away from the MRI scanner whereas online refers to the data acquired in the MRI chamber.

Note that, since only the high voltage - low current design was built into a prototype, all measurements and experimental results were gathered by this 3V design.

5.1 Offline Measurements

The offline measurements were an essential process in the design especially important for testing, debugging and checking operational details. These experiments required external devices which range from basic tools such as multimeters to extremely complex ones like network analyzers.

The simplest yet one of the most important measurement was DC biasing. Without proper current and voltage values, it was impossible to construct a working device. Furthermore, DC measurements turned out to be a good indicator to isolate a problem and to spot failed components. The DC measurements

were done by a no-name digital multimeter. The constructed circuit showed the DC values in Table 5.1, which mostly complied with the bias simulations.

Measurement	Value
V_{in}	2.85V
V_{laser}	0.93V
V_C	1.86V
V_{BE1}	0.816V
V_{CE1}	1.69V
I_{C1}	3.7mA
V_{BE2}	0.871V
V_{CE2}	1.653V
I_{C2}	12.3mA

Table 5.1: DC measurements of the transmitter using a multimeter

From these values, the overall power consumption could be calculated to be

$$P_{total} = 3V \cdot (3.7mA + 12.3mA) = 48mW. \tag{5.1}$$

In the above equation, AC component of the power was neglected, since the output RF power was very small even after amplification.

The second measurement was the insertion gain *S21*, which was for testing the signal path, including the amplifiers and E-O-E conversion. The instrument used for measurement was an HP/Agilent 8753D Vector Network Analyzer. Also, before any data acquisition takes place, full 2-port calibration had been performed for accuracy in the frequency range 63MHz to 65MHz. The power range was carefully adjusted to "-65 to -50dBm" with an active port power of -60dBm. This port power was an optimal value since higher levels saturated the device, and lower levels increased the uncertainty(noise) in the measurement. The resulting transmission data was viewed on a rectangular plot of S21(dB) versus frequency.

In the preliminary stages of design, the gain of the overall circuit was measured as 41dB, which indicated an amplifier gain of $41+19.6 = 60.6$dB. Later, problems associated with a high gain were observed and an intentional mismatch (non-optimal L-match) was created between the amplifier and laser diode to reduce gain. This modification decreased the gain to 33dB suggesting an amplifier gain of 52.6dB.

Making sure that the device had been correctly biased and successfully transmitting the RF signals, the next stage was to measure the noise figure. There were two methods to measure the noise figure but one was more accurate: Using a HP/Agilent 8970 Noise Figure Meter with HP/Agilent 346B Noise Source. Although this instrument is an automated, self calibrating system; it was available to us only at Aselsan Inc., Ankara. Casual measurements were done manually, using a Noise Source (HP/Agilent 346C) and HP/Agilent 8590L Spectrum Analyzer, as explained in the Appendix A.

Using Noise Figure Meter, the noise figure is recorded as 0.88dB,

$$NF = 0.88dB \tag{5.2}$$

with the amplifier connected to the original laser. The other method yields approximately the same results while considering the lack of calibration in our noise source

$$NF = 0.8dB. \tag{5.3}$$

Note that, the difference between $0.8dB$ and $0.88dB$ might be very difficult to observe, since ultra-low-noise measurements are very prone external noise sources such as antennas, EM reception on VHF band, nearby electronic devices and even power surges.

Later, when the laser was modified and corresponding noise levels increased, new measurements were required. They yield the similar results, indicating the gain in the preamplifiers were sufficient to boost the signals away from the higher noise levels,

$$NF = 0.91dB. \tag{5.4}$$

One final measurement, helpful in debugging the beginning of the amplifier was impedance measurement using HP/Agilent 8753D Vector Network Analyzer. The procedure was the same as insertion gain setup, with the same calibration and power properties. However, this time the measurements were *S11* and *Z11*,

in Smith Chart format and versus frequency. This test was especially useful in determining problems in the ULNA match circuitry, e.g. common failures of inductors and capacitors.

The measured impedance values were tabulated below, they closely matched simulation values.

	f MHz	S11 Mag	S11 Ang	Z11 R	Z11 X
Theoretical (3mA)	63	0.842	-93.52	8.0	-46.4j
Theoretical (3mA)	64	0.839	-96.06	7.9	-44.4j
Theoretical (4mA)	63	0.801	-99.71	9.3	-41.3j
Theoretical (4mA)	64	0.797	-102.42	9.2	-39.3j
Measured	64	0.853	-108.27	6.0	-35.8j

Table 5.2: S11 Parameter of the Transmitter, Theoretical vs. Measured

5.2 Online Measurements

Online experiments were performed in the Magnetic Resonance Imaging chamber using actual medical equipment. The MR device used throughout the experiments was a 1.5 Tesla device, manufactured by General Electric. In each experiment, there were at least two different measurements, one with the coil connected to a coaxial cable using active detuning; and the other with the fiber-optic system using passive detuning.

One point that should be observed is that, whenever fiber-optic system was used for interconnection, an attenuator had been placed between the receiver and internal amplifier of the MR scanner. This was a precaution not to saturate or harm the sensitive preamplifier of MRI instrument.

The imaging parameters were set to the values tabulated in Table 5.3 during the experiments.

In Table 5.3, $R1$ is the analog gain, $R2$ is the digital gain, f is excitation center frequency, TR is the recovery time, TE is the echo time and FOV is the

MR Imaging Parameter	Value
R1	13
R2	15
f	$63851735Hz$
Display Matrix	256×256
TR	$10000ms$
TE	$15.4ms$
FOV	$16cm \times 16cm$
Number of slices	7
Slice thickness	$3.5mm$

Table 5.3: MRI parameters during the experiments with 1.5T GE scanner.

field-of-view. There were other parameters missing here, transmit gain (T_G) and attenuator value (ATN), which were varied among the measurements. The object to be scanned was a phantom: a plastic bucket, filled with water $30cm$ deep with the coil inside a cylindrical gap in the middle of bucket.

The images in Figure 5.1 were acquired from the first experiments. As seen in the images, the preliminary transmission system showed a great amount of noise, indicating an problem in the first preamplifier or ultra-low-noise matching circuitry. Yet the images -although noisy- were proof of the successful transmission of signals.

In obtaining the images, the procedure was to connect the coil with a coaxial cable and obtain a 3-dimentional volumetric image from which the imaging parameters, including the Field-of-View(FOV) and number of slices were adjusted. Then an image was acquired using the same setup after which the coaxial was replaced with fiber-optic system and active tuning was converted to passive. Later, a series of measurements were done during which the level of attenuation was decreased step by step to acquire the best image.

In the later experiments, different modifications and corrections were done to the circuit to make it better: change of matching circuitry and adding shunt resistors to lower the gain, modifying the laser to make it MR-compatible, etc.

The resulting images from a later experiment is in Figure 5.2. As the pictures suggest, they were significant improvement compared to the preliminary ones.

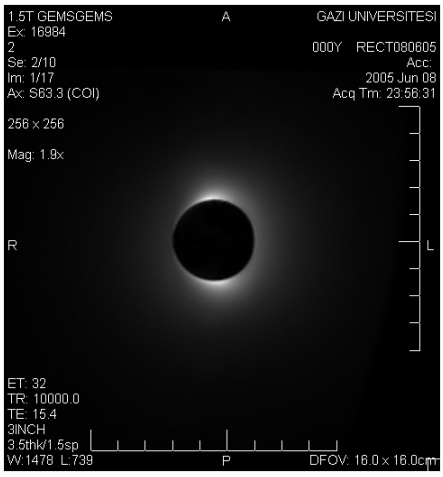

(a) Coaxial: $T_G = 122$

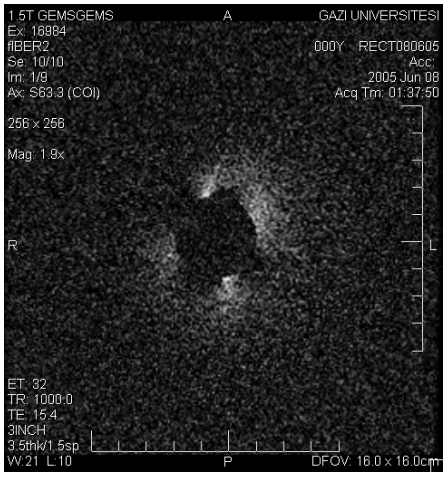

(b) Fiber Optic: $T_G = 122$, ATN: $30dB$

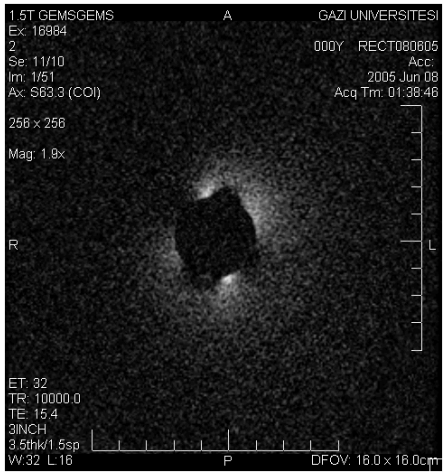

(c) Fiber Optic: $T_G = 122$, ATN: $10dB$

Figure 5.1: Images from the first experiment compared with the image from coaxial cable. These images are the proofs of principle, yet excessively noisy.

The SNR of the images are at the same order, even though connection through coaxial cable produced a better SNR (3 times the fiber-optic case).

However, there were problems associated with these images and their acquirement. During the experiments, the failure of the first transistor has been observed several times. It might be due to a failure in DC biasing, however a more possible reason would be a problem in the passive detuning circuitry.

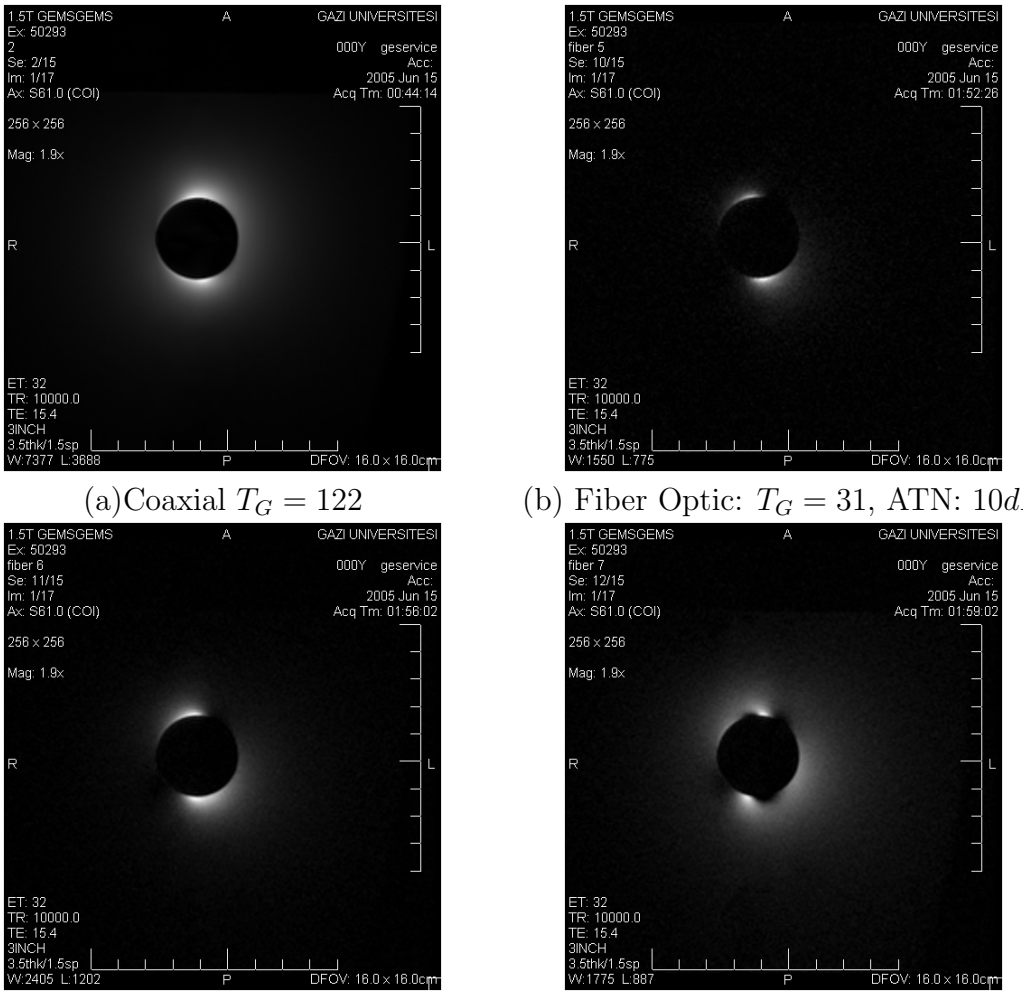

(a)Coaxial $T_G = 122$ (b) Fiber Optic: $T_G = 31$, ATN: $10dB$

(c) Fiber Optic: $T_G = 85$, ATN: $10dB$ (d) Fiber Optic: $T_G = 122$, ATN: $10dB$

Figure 5.2: Images from later experiments with better SNR.

- High power RF signals that can be intercepted through the excitation sample can burn the transistor slowly in the case of a detuning failure. Moreover, before the actual burning of transistor, it is fairly common to observe a fall in its low-noise performance [28]; which is what we had observed through the experiment process, seen as the extra noise in images.

- During scanning, manual prescanning was used to ensure that parameters stay the same in between experiments. Manual prescan presents a simple plot of the received signal: Throughout consecutive measurements the signal level continuously dropped in this plot; suggesting the burning of the

transistor was a long process similar to high-power accelerated aging.

- Furthermore, there was a loss of uniformity, observed even in the best images: The brightness around the coil was not as uniform as the coaxial case. This was another indicator pointing to the passive detuning.

Another interesting result rarely observed during these experiments was the acquisition of images with replicas, like the ones in Figure 5.3.

In these pictures, the replicas of the original image can be seen clearly. Unfortunately it is hard to explain these images; except that they were observed in correlation with the reduction of gain due to passive detuning. The replicas were in the *phase encoding* direction, which can be attributed to a sequence of events: Most logical explanation is the nonuniform sampling of the k-space in MRI scanner due to complex fast imaging algorithms. It is possible - and very likely - that MRI scanner traces the k-space in a complex fashion, compared to the line-by-line trace of the standard procedure. During this scanning the continuous reduction of gain in the preamplifier resulted in some Fourier series coefficients to be amplified less than others. It can be shown that replicas will symmetrically occur if the acquired k-space coefficients (a'_{kl}) are of the form

$$a'_{kl} = (1 + x\cos(-jk\frac{2\pi}{N}n_0))\ a_{kl} \tag{5.5}$$

where a_{kl} is the correct coefficients, k is the vertical index, l is the horizontal index, n_0 is the amount of vertical shift experienced by symmetrical replicas and x is an arbitrary coefficient ($|x| < 1$). The replicas were only possible if the scanner's k-space route and corresponding preamplifier gain at each horizontal line matched this coefficients. Comparing this with the replica images presented here, $n_0 \simeq 3N/8 = 96$.

The reason for failing to observe a better pattern in the generation of such images could be attributed to the more dominant effect: failure of transistor over time.

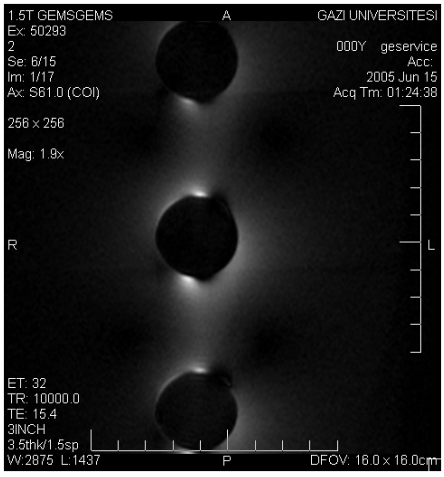

(a) Fiber Optic: $T_G = 31$, ATN: $20dB$

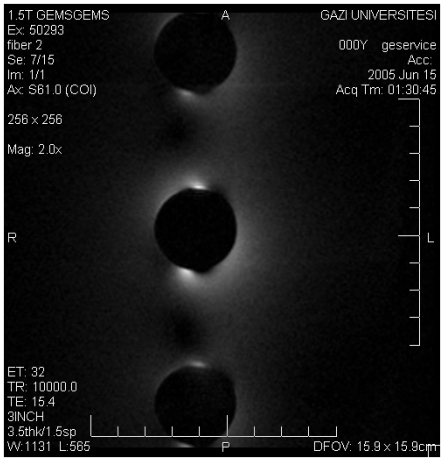

(b) Fiber Optic: $T_G = 31$, ATN: $10dB$

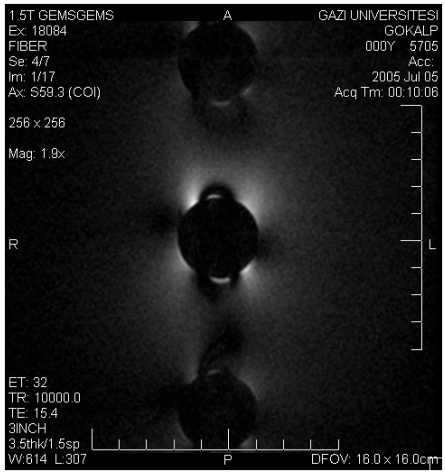

(c) Fiber Optic: $T_G = 126$, ATN: $30dB$

Figure 5.3: Images with replicas: The failure of passive decoupling.

Chapter 6

Discussions and Conclusion

During this project, a fiber optic MRI probe has been proposed, designed and developed. The aim of this work was to extend interventional imaging and parallel imaging techniques; both of which have promising future but suffer from the limitations of current technologies.

The prototype incorporates a fiber optic path to connect the coil to MRI scanner, through which the received MR signals are transmitted. Moreover, the probe is designed to be an ultra-low-noise system with minimal SNR degradation, which ensures the signals' integrity. Finally, the power consumption is low enough to be operated for several hours with a battery as small as the device.

The device was tested in a 1.5 Tesla GE MR scanner. Several images have been acquired which have SNR values comparable to images obtained by coaxial cables. The images also showed indicators to the erroneous parts of the device and have led to modifications in the prototype for better images.

The first problem was in the laser itself: The malfunction of the optical isolator and its effects to the image degradation. It is shown that optical isolators are of magnetic nature, and their use in MRI may result in both functional and physical problems. Functionally, a significant reduction of SNR is very possible; physically the misalignment of isolator due to strong external magnetic field may

block the optical path. Therefore, the isolator was removed even though this leads to increased laser intensity noise.

Another problem that the images suggest was the failure of passive decoupling. First, the ineffective passive decoupling resulted in the loss of uniformity of the main B_0 field. This effect showed itself as overly bright or dim spots in the images when compared to the ones gathered with coaxial cables. A consequence of this failure was the increased amount of RF power fed to the sensitive preamplifier; worsening its low noise characteristics over time and eventually burning the preamplifier.

The solution to the collapse of passive detuning is to use active detuning. However this requires dedicated control mechanism with precise timing. Fortunately, MRI scanners are equipped with this circuitry and its effect can be transmitted to the coil via an extra fiber. Moreover, the control fiber which is already present in current prototype can be modified to a 3-state design involving the control of active detuning besides switching the transmitter, eliminating the need for a separate fiber for active detuning. Using active decoupling with 3-state power and control circuitry will solve the problems due to passive decoupling; and increase the lifetime of the device considerably.

Although the fiber optic probe has great advantages over coaxial cabling, there are also possible disadvantages associated with the device. The biggest problem is the increased complexity: The fiber optic probe has significantly more components and a more complex circuitry compared to a simple coaxial cable; which makes it more prone to failures. Another problem is the nonlinearities: Since the device is designed to transmit low-power signals, feeding it with higher levels may compress the signals, saturate the device or break the small-signal assumption on the laser diode, resulting in the distortion of the MRI signals. Note that none of these nonlinearities are present in coaxial cables.

There are some possible enhancements to the prototype which can increase the benefits greatly. Considering parallel imaging, addition of frequency division multiplexing (FDM) of different channels is a nice improvement: It eliminates the need for a dedicated laser and fiber optic line for each channel, decreasing

the size, power consumption and cost significantly. Although there are possible problems with this configuration such as the intermodulation caused by nonlinearity; they can be avoided with optimization of channels per laser and clever design techniques.

The most beneficial improvement for interventional imaging would be the reduction of size. Integrated circuit solutions with embedded laser diode are possible, which can decrease the size substantially - even to the small size required for intravascular applications. Furthermore, photovoltaic power converters can be used to supply power externally with a laser rather than using a bulky battery; making the prototype virtually microscopic. Another enhancement would be to lower power consumption: Reduction of power consumption not only means smaller battery sizes, but it may also enable the use of smaller power generation devices such as piezoelectric material which can convert mechanical energy to electricity.

In parallel with the development of more demanding technologies of MRI, it is obvious that more sophisticated MRI scanners and probes will be designed and implemented. Our prototype was based to fulfill this emerging need and its proof of principle tests have been conducted successfully. Even though currently there are problems that should be solved before commercialization, this design and prototype is still a very strong candidate for the demanding needs of MRI.

Bibliography

[1] Ogan Ocali and Ergin Atalar. Intravascular magnetic resonance imaging using a loopless catheter antenna. *Magnetic Resonance in Medicine*, 37:112–118, 1997.

[2] Alastair J. Martin, Raymond F. McLoughlin, Kenneth C. Chu, Enzo A. Barberi, and Brian K. Rutt. An expandable intravenous rf coil for arterial wall imaging. *Journal of Magnetic Resonance Imaging*, 8:226–234, 1998.

[3] Kendrick A. Shunk, Joao A.C. Lima, Alan W. Heldman, and Ergin Atalar. Transesophageal magnetic resonance imaging. *Magnetic Resonance in Medicine*, 41:722–726, 1999.

[4] Harald H. Quick, Jean-Michael Serfaty, Harpreet K. Pannu, Rene Genadry, Christopher J. Yeung, and Ergin Atalar. Endourethral mri. *Magnetic Resonance in Medicine*, 45:138–146, 2001.

[5] Mitchell D. Schnall, Robert E. Lenkinski, Howard M. Pollack, Yutaka Imai, and Herbert Y. Kressel. Prostate: Mr imaging with an endorectal surface coil. *Radiology*, 172:570–574, 1989.

[6] Gabor Fichtinger, Axel Krieger, Robert C. Susil, Atilla Tanacs, Louis L. Whitcomb, and Ergin Atalar. Transrectal prostate biopsy inside closed mri scanner with remote actuation, under real-time image guidance. *Medical Image Computing and Computer-Assisted Intervention-Miccai 2002.*, 1:91–98, 2002.

[7] Maurits Konings, Lambertus W. Bartels, Henk F.M. Smits, and Chris J.G. Bakker. Heating around intravascular guidewires by resonating rf waves. *Journal of Magnetic Resonance Imaging*, 12:79–85, 2000.

[8] Wolfgang R. Nitz, Arnulf Oppelt, Wolfgang Renz, Christoph Manke, Markus Lenhart, and Johann Link. On the heating of linear conductive structures as guide wires and catheters in interventional mri. *Journal of Magnetic Resonance Imaging*, 13:105–114, 2001.

[9] Christina Armenean, Emmanuel Perrin, Mircea Armenean, Olivier Beuf, Frank Pilleul, and Hervé Saint-Jalmes. Rf-induced temperature elevation along metallic wires in clinical magnetic resonance imaging: Influence of diameter and length. *Magnetic Resonance in Medicine*, 52:1200–1206, 2004.

[10] Christopher J. Yeung, Robert C. Susil, and Ergin Atalar. Rf safety of wires in interventional mri: Using a safety index. *Magnetic Resonance in Medicine*, 47:187–193, 2002.

[11] Mark E. Ladd and Harald H. Quick. Reduction of resonant rf heating in intravascular catheters using coaxial cables. *Magnetic Resonance in Medicine*, 43:615–619, 2000.

[12] S. Weiss, P. Vernickel, T. Schaeffter, V. Schulz, and B. Gleich. A safe transmission line for interventional devices. In *Proceedings of the 5th Interventional MRI Symposium*, http://www.uni-leipzig.de/ radiol/start/archiv/5thinterventional/Abstracts.htm, 2004.

[13] Frank K. Wacker, Klaus Reither, Gordian Branding, Michael Wendt, and Karl-Jürgen Wolf. Magnetic resonance-guided vascular catheterization: Feasibility using a passive tracking technique at 0.2 telsa in a pig model. *Journal of Magnetic Resonance Imaging*, 10:841–844, 1999.

[14] E. Y. Wong, Q. Zhang, J. L. Duerk, J. S. Lewin, and M. Wendt. An optical system for wireless detuning of parallel resonant circuits. *Magnetic Resonance in Medicine*, 12:632–638, 2000.

[15] G. C. Wiggins, C. Triantafyllou, A. Potthast, A. Reykowski, M. Nittka, and L. L. Wald. A 32 channel receive-only phased array coil for 3t with novel geodesic tiling geometry. In *Proceedings of the International Society of Magnetic Resonance in Medicine 13th Scientific Meeting (ISMRM'05)(CD-ROM)*, 2005.

[16] V. Matschl, A. Reykowsky, K. Jahns, M. Hergt, and H. Fischer. 48 channel body/spine matrix coils fot 3 tesla. In *Proceedings of the International Society of Magnetic Resonance in Medicine 13th Scientific Meeting (ISMRM'05)(CD-ROM)*, 2005.

[17] G. C. Wiggins, A. Potthast, C. Triantafyllou, F. Lin, T. Benner, C. J. Wiggins, and L. Wald. A 96-channel mri system with 23- and 90-channel phase array head coils at 1.5 tesla. In *Proceedings of the International Society of Magnetic Resonance in Medicine 13th Scientific Meeting (ISMRM'05)(CD-ROM)*, 2005.

[18] G. P. Koste, M. C. Neilsen, T. R. Tolliver, R. L. Frey, and R.D. Watkins. Optical mr receive coil array interconnect. In *Proceedings of the International Society of Magnetic Resonance in Medicine 13th Scientific Meeting (ISMRM'05)(CD-ROM)*, 2005.

[19] Omer G. Memis, Orhan Aytur, and Ergin Atalar. Optical transmission of mri signals: A safe alternative for internal mri probes. In *Proceedings of the European Society of Magnetic Resonance in Medicine and Biology 20th Scientific Meeting (ESMRMB'03)(CD-ROM)*, 2003.

[20] Bahaa E. A. Saleh and Malvin Carl Teich. *Fundamentals of Photonics*. Wiley, New York, 1991.

[21] David K. Cheng. *Field and Wave Electromagnetics*. Addison-Wesley Publishing Company, USA, 1992.

[22] Dwight G. Nishimura. *Principles of Magnetic Resonance Imaging*. Dwight G. Nishimura, California, 1996.

[23] Reinhold Ludwig and Pavel Bretchko. *RF Circuit Design: Theory and Applications*. Prentice Hall, Upper Saddle River, NJ, 2000.

[24] Rick Core. Pin-limiter diodes effectively protect receivers. http://www.edn.com/article/CA486567.html, 2004.

[25] W. A. Edelstein, C. J. Hardy, and O. M. Muller. Electronic decoupling of surface-coil receivers for nmr imaging and spectroscopy. *Journal of Magnetic Resonance*, 67:156–161, 1985.

[26] Guillermo Gonzales. *Microwave Transistor Amplifiers: Analysis and Design*. Prentice Hall, Upper Saddle River, NJ, 1997.

[27] Donald A. Neamen. *Electronic Circuit Analysis and Design*. McGraw Hill, New York, NY, 2001.

[28] Peter Vizmuller. *RF Design Guide: Systems, Circuits and Equations*. Artech House Inc., Norwood ,MA, 1995.

Appendix A

Noise Figure Measurement

Identifying and describing the sources of noise is not enough to characterize a device according to its noise. Its noise factor and noise figures are used as the noise related parameters of the device. Together with the gain, these parameters are enough to calculate how noisy an actual system is.

Noise figure is defined using the concept of noise temperature, in which every noise source is treated as if it is a resistor with a specific temperature. In the definition of thermal noise, the available power from a resistor on a matched load is given by

$$P_{th} = k_B T_N B, \tag{A.1}$$

where T_N is defined to be the temperature of the resistor. Extending the definition, T_N becomes the noise temperature of any arbitrary noise source, calculated to yield the calibrated noise power when entered to the equation above. In connection, the Excess Noise Ratio (ENR) of a noise source is defined as

$$ENR = \frac{T_N}{290} - 1, \tag{A.2}$$

which is used to find T_N and its corresponding noise power P_{Th}. ENR is frequently used in calibrated noise sources, which are used in noise figure measurements. The

noise factor and noise figure of a noisy system is

$$Noise\ factor: \quad F = \frac{T_N}{290} + 1, \tag{A.3}$$

$$Noise\ figure: \quad NF = 10\log(\frac{T_N}{290} + 1). \tag{A.4}$$

Another important relationship often used in the calculation of noise figure is

$$F_{Total} = F_1 + \frac{F_2 - 1}{G_1} + ... + \frac{F_m - 1}{G_1 G_2 ... G_{m-1}} \tag{A.5}$$

and it is used to calculate the total noise factor (also corresponding noise figure) of a cascade of systems whose individual noise figures and gains are known. The setup for measurement of noise is shown in Fugure A.1

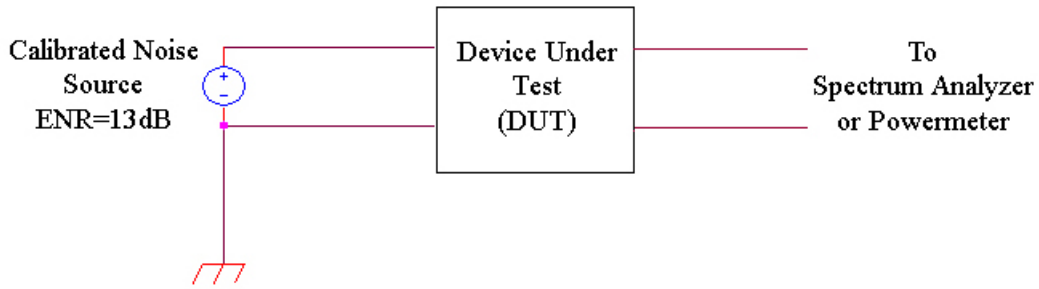

Figure A.1: Noise Figure measurement setup: *Device Under Test(DUT)* is placed in between calibrated noise source and a power measurement device.

The device under test (DUT) is placed between the noise source and the analyzer. The noise source is at the left end of the circuit and two measurements are done, with the noise source on and off. The noise source has an ENR (Excess Noise Ratio) of $13dB$ which corresponds to $6076K$ noise temperature by the relationship

$$T_{ENR} = (10^{13/10} + 1) \cdot T_0 = 6076K, \tag{A.6}$$

where $T_0 = 290K$. The analyzer at the right end can be a powermeter or a spectrum analyzer. The spectrum analyzer is our weapon of choice, as it is frequency adjustable and is more customizable.

As stated before, there are two measurements to be done when measuring the noise figure, one with the noise source on and the other off. Corresponding

equations are

$$P_1 = G_T \cdot (k_B T_H B + P_{N,T}), \tag{A.7}$$

$$P_2 = G_T \cdot (k_B T_L B + P_{N,T}). \tag{A.8}$$

Note that T_H and T_L are associated with the noise source and T_N is the noise temperature of the system whose noise figure is to be measured. Then the explicit formula of F, using the measured powers is

$$\frac{P_1}{P_2} = \frac{T_H + T_N}{T_L + T_N} \tag{A.9}$$

yielding

$$NF = ENR(dB) - 10log(Y - 1), \qquad Y = \frac{P_1}{P_2}. \tag{A.10}$$

Although this formula is an exact relationship with no approximations, in practice it is not easy to find the exact noise figure of a system, especially when the system is ultra-low noise: The circuit may act like a coil, receiving external noise; the external temperature T_0 may not exactly be $290K$ or the heat produced with the operation of system may undesirably shift the fundamental parameters.

Appendix B

Matching Data and Calculations

There are two matching circuits present in the design. The first is the ultra-low noise match preceding the amplifier; and the second is the match for maximum power transfer in between the preamplifier and laser diode. Both of these circuits contain a simple L-match topology, since the design is narrowband.

For the ultra-low noise match, it was required for the transistor to be loaded with an appropriate microwave load at the input port. This load is presented in the corresponding reflection (Γ_{opt}) at the datasheet of a transistor. The specific Γ_{opt} values for BFP420 is tabulated in Table B.1.

I_C -	f GHz	F_{min} dB	Γ_{opt} Mag	Γ_{opt} Ang	$r_n/50$ -
3.0mA	≤ 0.450	0.77	0.30	20	0.22
4.0mA	≤ 0.450	0.81	0.25	18	0.20

Table B.1: Γ_{opt} values for BFP420 transistor.

Considering that the coil was matched to 50Ω, the L-match circuits yielding the smallest inductor values are 82nH-27pF and 100nH-22pF.

The second L-match circuit was used in between the preamplifier and laser diode. The output impedance of the transistor (at $I_C = 12mA$) is very high (see Table 3.2) compared to the RF resistance of the laser diode (4-6Ω), therefore

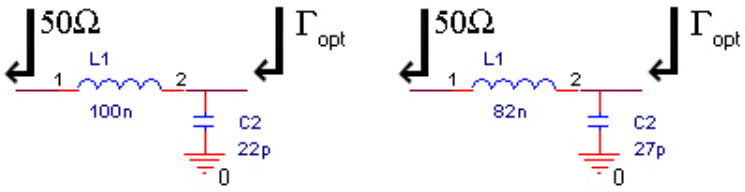

(a) (b)

Figure B.1: Schematics of the ultra-low noise match circuits, (a) 100nH-22pF, (b) 82nH-27pF

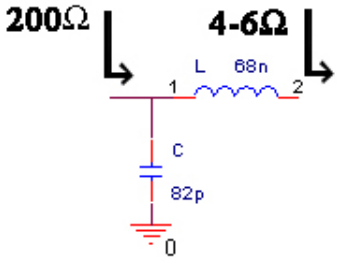

Figure B.2: Schematics of the L-match between the preamplifier and laser diode

matching was required for efficient power transfer. The matching circuit of 68nH-82pF transforms the input impedance of the laser diode from several Ohms to around 200Ω.

Note that interstage matching circuit was not used in the preamplifier; as the high output impedance of the first stage presented a good match to the high input impedance of the second stage.

Appendix C

BFP420 Transistor Datasheet

NPN Silicon RF Transistor

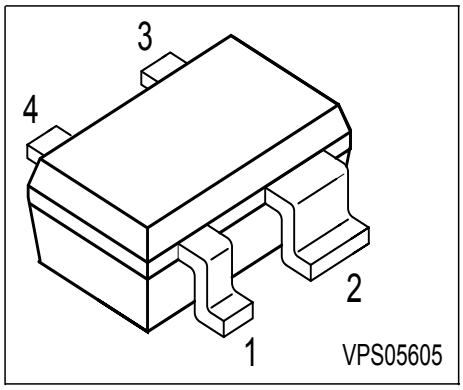

- For high gain low noise amplifiers
- For oscillators up to 10 GHz
- Noise figure F = 1.1 dB at 1.8 GHz
  outstanding G_{ms} = 21 dB at 1.8 GHz
- Transition frequency f_T = 25 GHz
- Gold metallization for high reliability
- **SIEGET ® 25** GHz f_T - **Line**

ESD: **E**lectro**s**tatic **d**ischarge sensitive device, observe handling precaution!

Type	Marking	Pin Configuration				Package
BFP420	AMs	1 = B	2 = E	3 = C	4 = E	SOT343

Maximum Ratings

Parameter	Symbol	Value	Unit
Collector-emitter voltage	V_{CEO}	4.5	V
Collector-base voltage	V_{CBO}	15	
Emitter-base voltage	V_{EBO}	1.5	
Collector current	I_C	35	mA
Base current	I_B	3	
Total power dissipation $T_S \leq 107°C$ 1)	P_{tot}	160	mW
Junction temperature	T_j	150	°C
Ambient temperature	T_A	-65 ... 150	
Storage temperature	T_{stg}	-65 ... 150	

Thermal Resistance

Junction - soldering point2)	R_{thJS}	≤ 260	K/W

1T_S is measured on the emitter lead at the soldering point to the pcb

2For calculation of R_{thJA} please refer to Application Note Thermal Resistance

Electrical Characteristics at T_A = 25°C, unless otherwise specified.

Parameter	Symbol	Values			Unit
		min.	typ.	max.	
DC characteristics					
Collector-emitter breakdown voltage I_C = 1 mA, I_B = 0	$V_{(BR)CEO}$	4.5	5	-	V
Collector-base cutoff current V_{CB} = 5 V, I_E = 0	I_{CBO}	-	-	200	nA
Emitter-base cutoff current V_{EB} = 1.5 V, I_C = 0	I_{EBO}	-	-	35	µA
DC current gain I_C = 20 mA, V_{CE} = 4 V	h_{FE}	50	100	150	-
AC characteristics (verified by random sampling)					
Transition frequency I_C = 30 mA, V_{CE} = 3 V, f = 2 GHz	f_T	18	25	-	GHz
Collector-base capacitance V_{CB} = 2 V, f = 1 MHz	C_{cb}	-	0.15	0.3	pF
Collector-emitter capacitance V_{CE} = 2 V, f = 1 MHz	C_{ce}	-	0.37	-	
Emitter-base capacitance V_{EB} = 0.5 V, f = 1 MHz	C_{eb}	-	0.55	-	
Noise figure I_C = 5 mA, V_{CE} = 2 V, Z_S = Z_{Sopt} , f = 1.8 GHz	F	-	1.1	-	dB
Power gain, maximum stable [1)] I_C = 20 mA, V_{CE} = 2 V, Z_S = Z_{Sopt} , Z_L = Z_{Lopt} , f = 1.8 GHz	G_{ms}	-	21	-	
Insertion power gain I_C = 20 mA, V_{CE} = 2 V, f = 1.8 GHz, Z_S = Z_L = 50Ω	$\|S_{21}\|^2$	14	17	-	
Third order intercept point I_C = 20 mA, V_{CE} = 2 V, Z_S=Z_{Sopt} , Z_L=Z_{Lopt} , f = 1.8 GHz	IP_3	-	22	-	dBm
1dB Compression point I_C = 20 mA, V_{CE} = 2 V, f = 1.8 GHz, Z_S=Z_{Sopt} , Z_L=Z_{Lopt}	P_{-1dB}	-	12	-	

[1] $G_{ms} = |S_{21} / S_{12}|$

SPICE Parameters (Gummel-Poon Model, Berkley-SPICE 2G.6 Syntax) :

Transistor Chip Data

IS =	0.20045	fA	BF =	72.534	-	NF =	1.2432	-
VAF =	28.383	V	IKF =	0.48731	A	ISE =	19.049	fA
NE =	2.0518	-	BR =	7.8287	-	NR =	1.3325	-
VAR =	19.705	V	IKR =	0.69141	A	ISC =	0.019237	fA
NC =	1.1724	-	RB =	8.5757	Ω	IRB =	0.72983	mA
RBM =	3.4849	Ω	RE =	0.31111		RC =	0.10105	Ω
CJE =	1.8063	fF	VJE =	0.8051	V	MJE =	0.46576	-
TF =	6.7661	ps	XTF =	0.42199	-	VTF =	0.23794	V
ITF =	1	mA	PTF =	0	deg	CJC =	234.53	fF
VJC =	0.81969	V	MJC =	0.30232	-	XCJC =	0.3	-
TR =	2.3249	ns	CJS =	0	F	VJS =	0.75	V
MJS =	0	-	XTB =	0	-	EG =	1.11	eV
XTI =	3	-	FC =	0.73234	-	TNOM	300	K

C'-E'-Diode Data (Berkley-SPICE 2G.6 Syntax) :

IS =	3.5	fA	N =	1.02	-	RS =	10	Ω

All parameters are ready to use, no scaling is necessary

Package Equivalent Circuit:

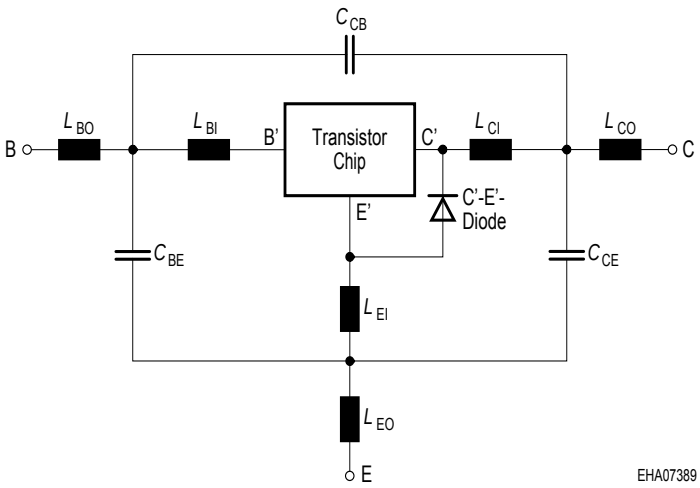

L_{BI} =	0.47	nH
L_{BO} =	0.53	nH
L_{EI} =	0.23	nH
L_{EO} =	0.05	nH
L_{CI} =	0.56	nH
L_{CO} =	0.58	nH
C_{BE} =	136	fF
C_{CB} =	6.9	fF
C_{CE} =	134	fF

Valid up to 6GHz

The SOT-343 package has two emitter leads. To avoid high complexity of the package equivalent circuit, both leads are combined in one electrical connection.

Extracted on behalf of Infineon Technologies AG by:
Institut für Mobil-und Satellitentechnik (IMST)

For examples and ready to use parameters please contact your local Infineon Technologies distributor or sales office to obtain a Infineon Technologies CD-ROM or see Internet:
http://www.infineon.com/silicondiscretes

Aug-20-2001

For non-linear simulation:

- Use transistor chip parameters in Berkeley SPICE 2G.6 syntax for all simulators.
- If you need simulation of the reverse characteristics, add the diode with the C'-E'- diode data between collector and emitter.
- Simulation of package is not necessary for frequencies < 100MHz. For higher frequencies add the wiring of package equivalent circuit around the non-linear transistor and diode model.

Note:

- This transistor is constructed in a common emitter configuration. This feature causes an additional reverse biased diode between emitter and collector, which does not effect normal operation.

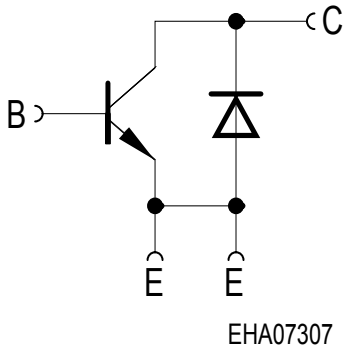

Transistor Schematic Diagram

The common emitter configuration shows the following advantages:

- Higher gain because of lower emitter inductance.
- Power is dissipated via the grounded emitter leads, because the chip is mounted on copper emitter leadframe.

Please note, that the broadest lead is the emitter lead.

Common Emitter S- and Noise-parameter

For detailed S- and Noise-parameters please contact your local Infineon Technologies distributor or sales office to obtain a Infineon Technologies Application Notes CD-ROM or see Internet: http://www.infineon.com/silicondiscretes

Total power dissipation $P_{tot} = f(T_S)$

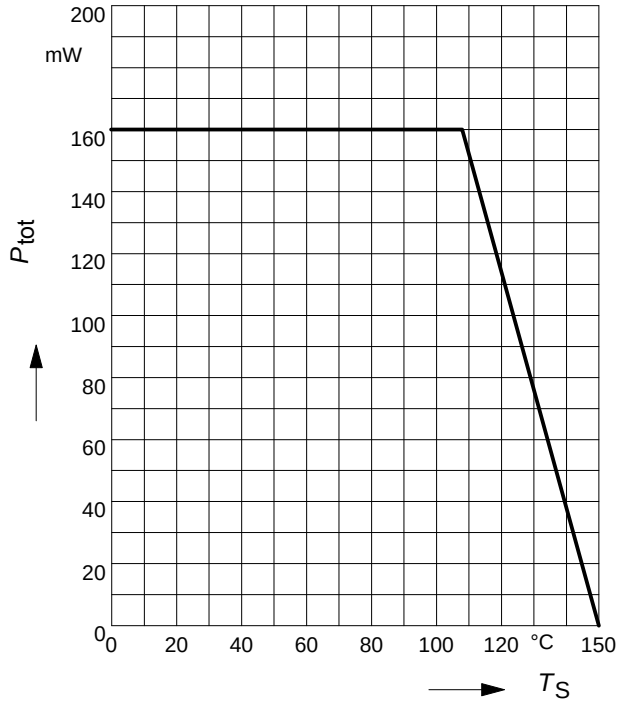

Transition frequency $f_T = f(I_C)$

f = 2 GHz

V_{CE} = parameter in V

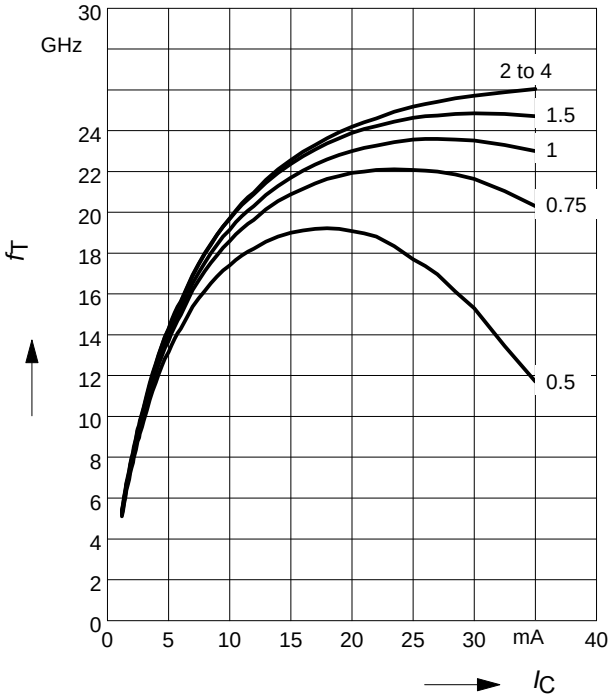

Permissible Pulse Load $R_{thJS} = f(t_p)$

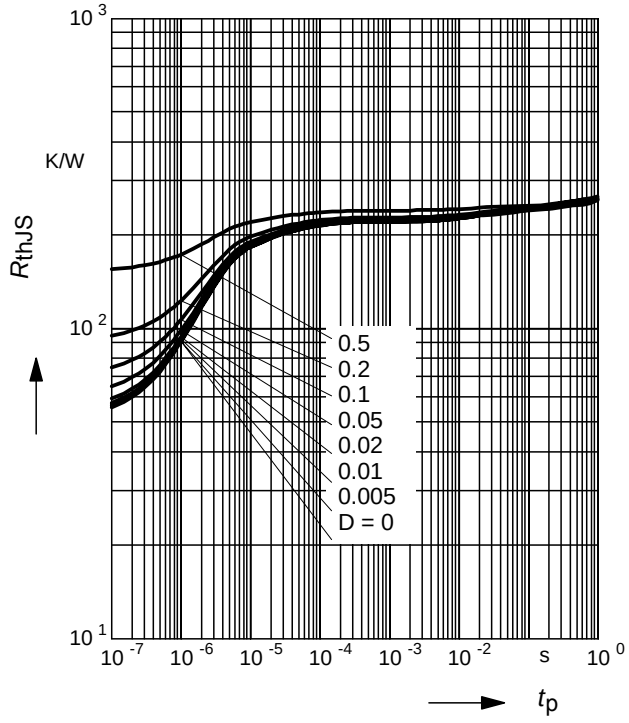

Permissible Pulse Load

$P_{totmax}/P_{totDC} = f(t_p)$

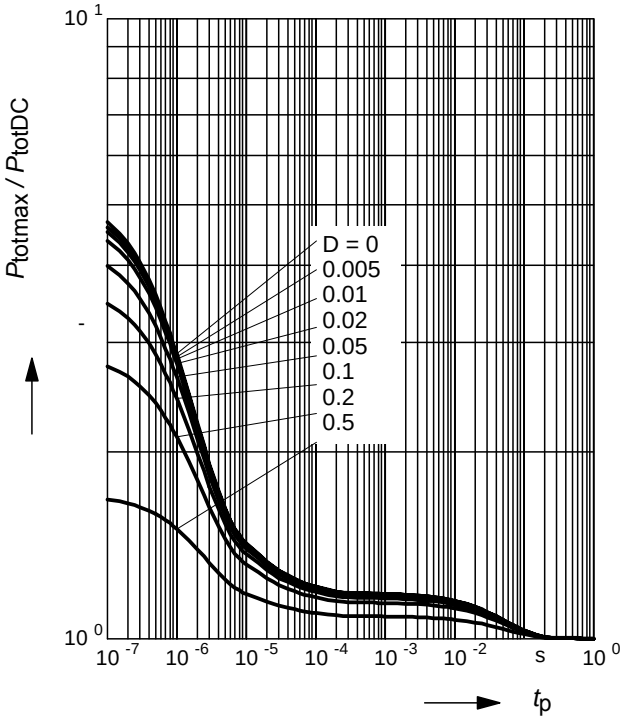

Power gain G_{ma}, G_{ms}, $|S_{21}|^2 = f(f)$
V_{CE} = 2V, I_C = 20 mA

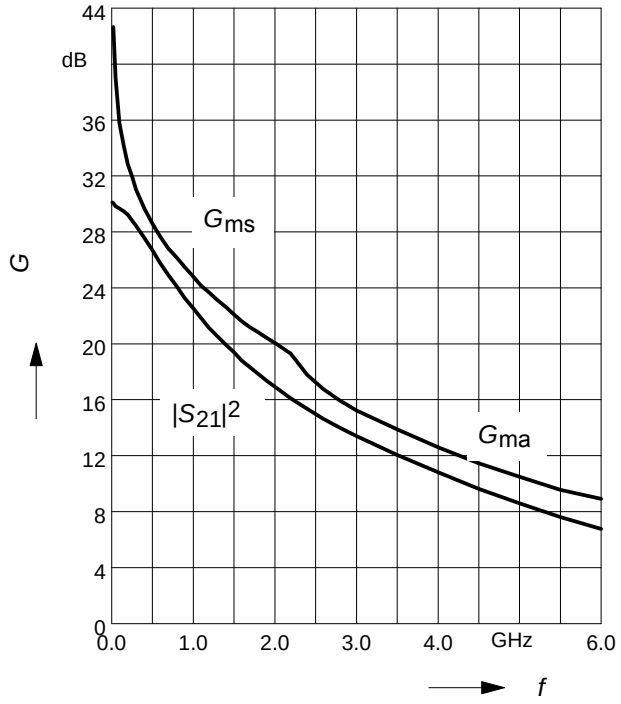

Power gain G_{ma}, $G_{ms} = f(I_C)$
V_{CE} = 2V
f = parameter in GHz

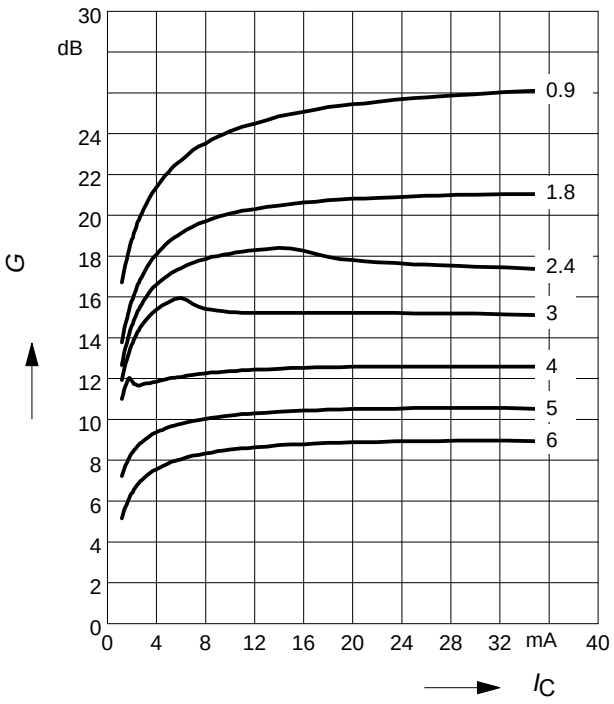

Power gain G_{ma}, $G_{ms} = f(V_{CE})$
I_C = 20 mA
f = parameter in GHz

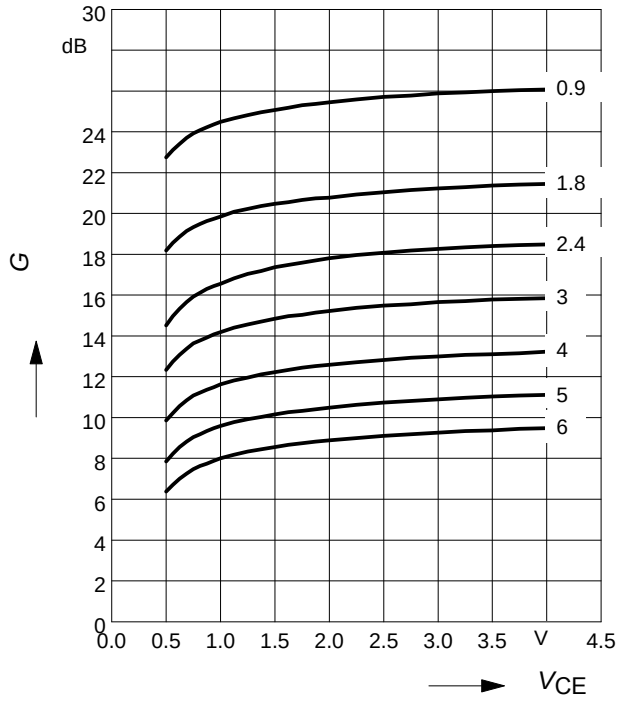

Collector-base capacitance $C_{cb} = f(V_{CB})$
f = 1MHz

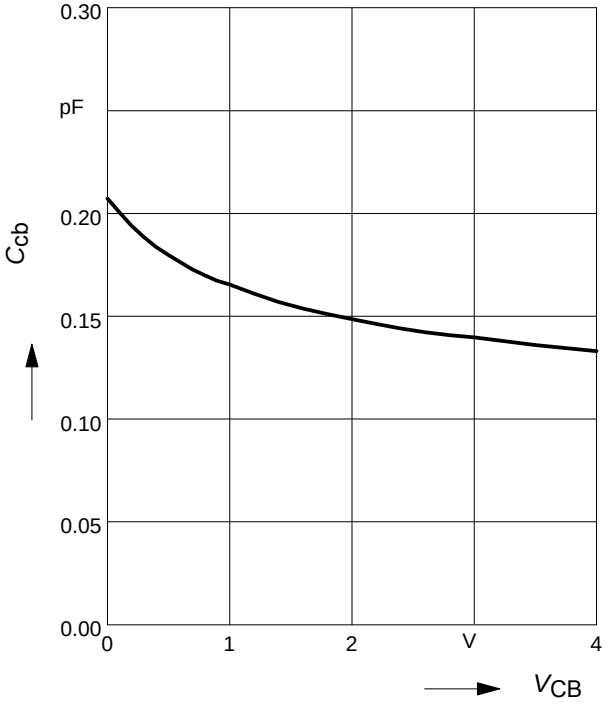

Noise figure $F = f(I_C)$
V_{CE} = 2 V, $Z_S = Z_{Sopt}$

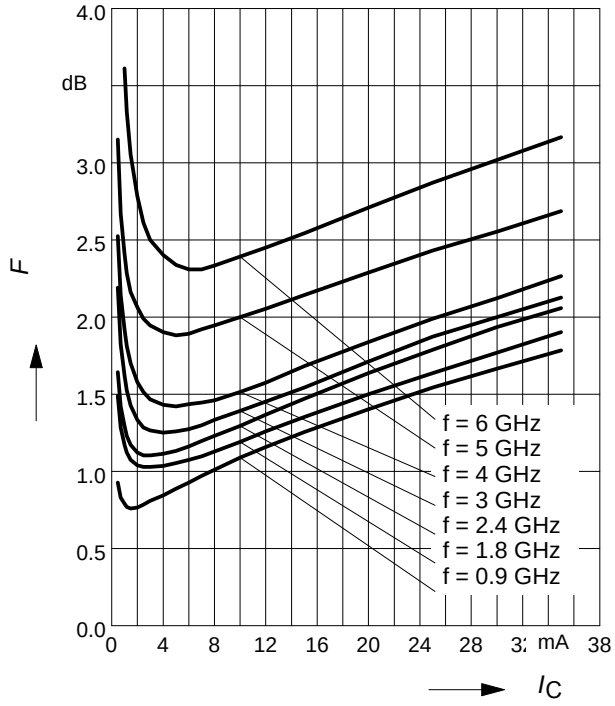

Noise figure $F = f(I_C)$
V_{CE} = 2 V, f = 1.8 GHz

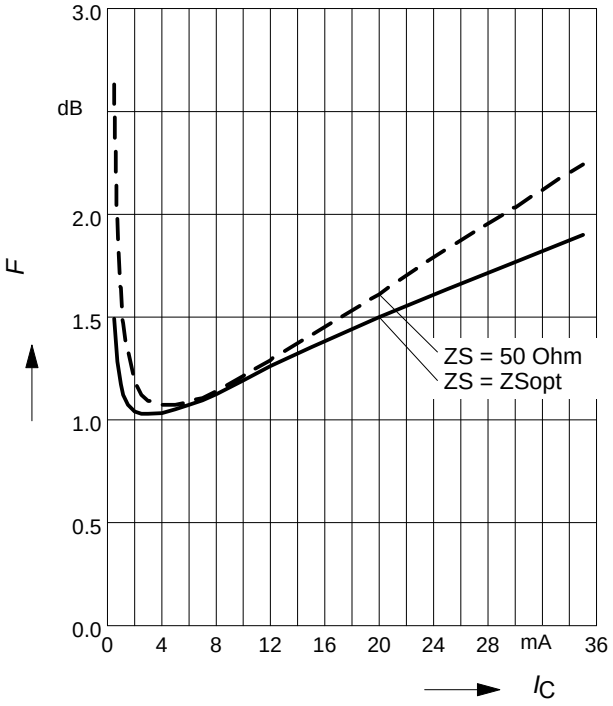

Noise figure $F = f(f)$
V_{CE} = 2 V, $Z_S = Z_{Sopt}$

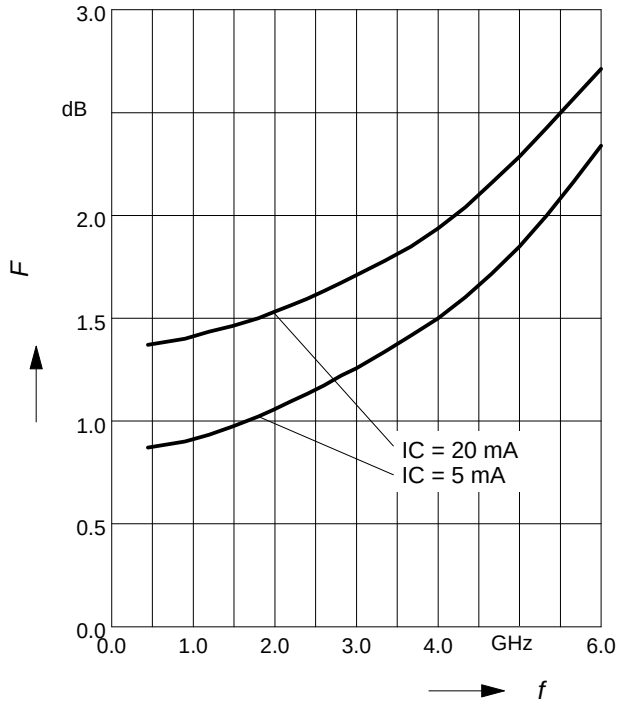

Source impedance for min.
Noise Figure versus Frequency
V_{CE} = 2 V, I_C = 5 mA / 20 mA

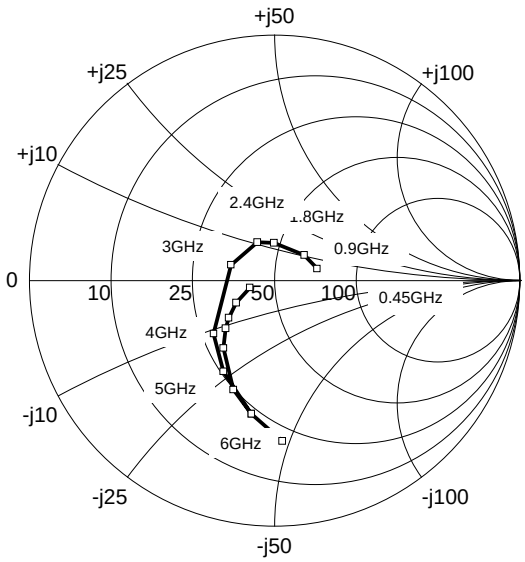

Package Outline

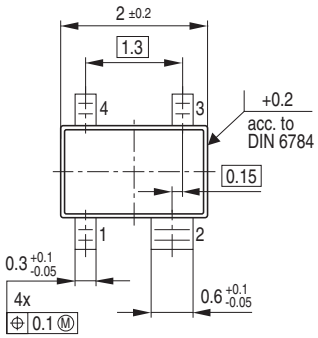

Foot Print

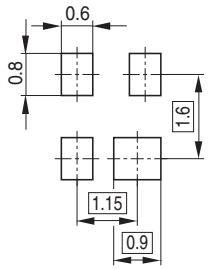

Marking Layout

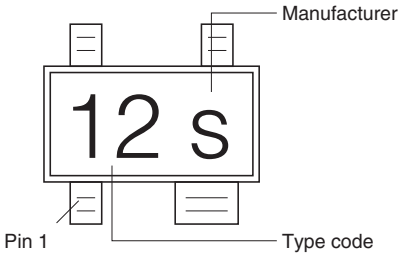

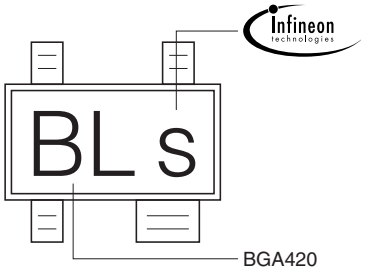

Example

Packing

Code E6327: Reel ø180 mm = 3.000 Pieces/Reel
Code E6433: Reel ø330 mm = 10.000 Pieces/Reel

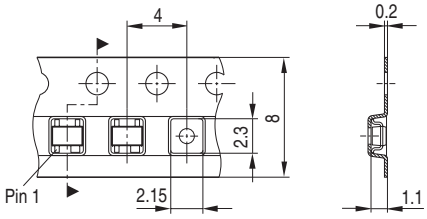

Published by Infineon Technologies AG,
St.-Martin-Strasse 53,
81669 München

Attention please!

The information herein is given to describe certain components and shall not be considered as a guarantee of characteristics.
Terms of delivery and rights to technical change reserved.
We hereby disclaim any and all warranties, including but not limited to warranties of non-infringement, regarding circuits, descriptions and charts stated herein.

Information

For further information on technology, delivery terms and conditions and prices please contact your nearest Infineon Technologies Office (www.Infineon.com).

Warnings

Due to technical requirements components may contain dangerous substances. For information on the types in question please contact your nearest Infineon Technologies Office.
Infineon Technologies Components may only be used in life-support devices or systems with the express written approval of Infineon Technologies, if a failure of such components can reasonably be expected to cause the failure of that life-support device or system, or to affect the safety or effectiveness of that device or system. Life support devices or systems are intended to be implanted in the human body, or to support and/or maintain and sustain and/or protect human life. If they fail, it is reasonable to assume that the health of the user or other persons may be endangered.

Appendix D

Laser Diode Datasheet

APPLIED OPTOELECTRONICS, INC.

AOI 1550nm DFB Laser Test Data

P/N: DFB-1550-C5-2-A-SA-A-A-02
S/N: 03002651

Parameter	Unit	Operating Temp. 25°C
Threshold Current	mA	13.54
Optical Output Power	mW	2.00
Slope Efficiency	mW/mA	0.11
Operating Current*	mA	31.21
Monitor Current*	μA	81.50
OMI	%	10.00
IMD2**	dBc	-54.34
IMD3**	dBc	-73.29
RIN @ 300MHz	dB/Hz	153.64
CNR(T-8)	dB	61.45

* steady state
** 13MHz and 19MHz 2-tone measurement

Spectrum

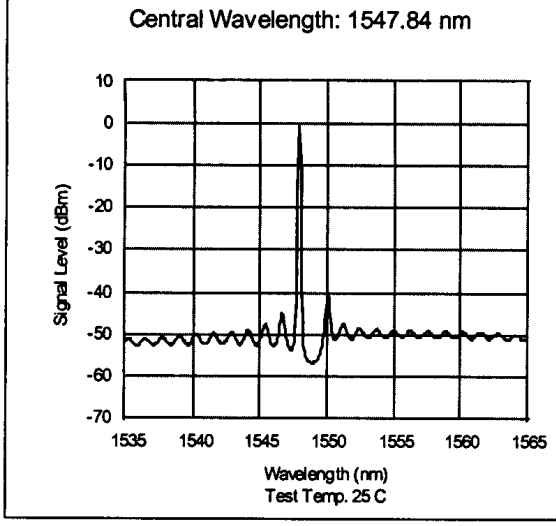

Pin Assignment

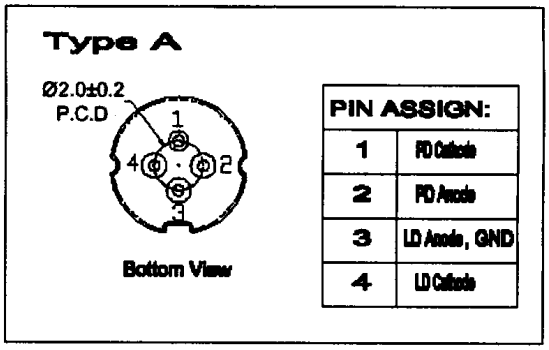

Test Date: March 10, 2004 **Testing:**_____